DCE-MRI in assessment of tumor hypoxia, radiation response, and metastatic potential

by

Kirsti Marie Øvrebø

Radiation Biology and Tumor Physiology Group, Department of Radiation Biology,
Institute for Cancer Research, The Norwegian Radium Hospital, Oslo University Hospital

© Kirsti Marie Øvrebø, 2013

Series of dissertations submitted to the
Faculty of Mathematics and Natural Sciences, University of Oslo
No. 1286

ISSN 1501-7710

All rights reserved. No part of this publication may be
reproduced or transmitted, in any form or by any means, without permission.

Cover: Inger Sandved Anfinsen.
Printed in Norway: AIT Oslo AS.

Produced in co-operation with Akademika publishing.
The thesis is produced by Akademika publishing merely in connection with the thesis defence. Kindly direct all inquiries regarding the thesis to the copyright holder or the unit which grants the doctorate.

ACKNOWLEDGMENTS

The work presented here was carried out in the Department of Radiation Biology, Institute for Cancer Research, The Norwegian Radium Hospital, Oslo University Hospital during the years 2009-2012. Financial support was provided by the South-Eastern Norway Regional Health Authority. This support is gratefully acknowledged.

Firstly, I want to thank my supervisor, Professor Einar K. Rofstad, for giving me the opportunity to work in his research group. His advice and support have been invaluable.

I would also like to thank all my co-authors for fruitful collaboration, in particular Christine Ellingsen, Kristine Gulliksrud and Tord Hompland. My gratitude also goes to all other colleagues of the Radiation Biology and Tumor Physiology Group.

I am grateful to the Radiological Department at the Norwegian Radium Hospital for facilitating my work in the MR-laboratory.

I extend my thanks to all my friends for supporting me, and for understanding when work has made me less available to them. Special thanks must go to Marit Flinder Johannessen and Ewa K. Schage for daily motivation.

Finally, I offer my thanks to my parents and my brother for supporting me all the way and, last but not least, to my dear Richard for believing in me.

Oslo 2012

Kirsti Marie Øvrebø

ABSTRACT

Hypoxia in tumors has been found to decrease the effectiveness of cancer treatment; in particular, it can diminish the effect of radiation therapy. Furthermore, hypoxia has been associated with malignant progression and metastatic disease. Patients with hypoxic tumors may thus benefit from a more aggressive treatment. A noninvasive diagnostic method for detecting these tumors is therefore urgently needed.

In this thesis, the potential usefulness of dynamic Gd-DTPA-enhanced MRI for assessing tumor hypoxia, radiation response, and metastatic potential has been evaluated preclinically. The DCE-MRI series were analyzed by using one of the most widely known pharmacokinetic models, the generalized kinetic model of Tofts. Human melanoma xenografts and cervical carcinoma xenografts were used as tumor models in the study. The DCE-MRI-derived parameters K^{trans} and v_e were shown to be able to distinguish between tumors with and without hypoxia, as well as to give information about the extent of tumor hypoxia. Furthermore, it was demonstrated that K^{trans} is able to predict radiation response. Finally, both K^{trans} and v_e showed the ability to predict metastatic potential. In conclusion, this preclinical study demonstrates the potential of the DCE-MRI-derived parameters K^{trans} and v_e as predictive markers, warranting further clinical studies.

CONTENTS

AIMS OF THE STUDY

Approximately 50 years ago, Thomlinson and Gray proposed that there were regions of low levels of oxygen, hypoxic tissue, in human tumors (Thomlinson and Gray, 1955). More recent clinical investigations have revealed that there are hypoxic regions in a wide range of malignancies, including: cancers of the breast, uterine cervix, vulva, head and neck, prostate, rectum, pancreas, and lung, and also brain tumors, soft tissue sarcomas, non-Hodgkin's lymphomas, malignant melanomas, metastatic liver tumors, and renal cancer (Vaupel and Mayer, 2007; Wouters et al., 2002). Clinical studies have shown that tumor hypoxia is a prognostic marker independent of other prognostic factors such as tumor stage and nodal status (Vaupel and Mayer, 2007). Additionally, tumor hypoxia may cause resistance to treatment and promote metastatic spread (Wouters et al., 2002). Patients with extensive hypoxic tumors may therefore benefit from receiving a particularly aggressive treatment. A noninvasive method for identifying these patients is therefore urgently needed.

Dynamic contrast-enhanced magnetic resonance imaging (DCE-MRI) is a noninvasive imaging technique that is currently being used in oncology for cancer detection, staging, diagnosis, and assessment of treatment response (Hylton, 2006; Zahra et al., 2007). Several studies have found correlations between DCE-MRI-derived parameters and known prognostic factors such as histological grade, lymph node status, and presence of metastatic disease (Hylton, 2006). Studies have also suggested that DCE-MRI may provide useful prognostic information for cancer patients receiving radiotherapy (Zahra et al., 2007). Additionally, clinical studies have suggested that valid information about the hypoxic status of the tumor can be obtained by DCE-MRI (Cooper et al., 2000; Newbold et al., 2009).

The potential of gadolinium diethylene-triamine penta-acetic acid (Gd-DTPA)-based DCE-MRI-derived parameters as biomarkers for particularly aggressive tumors is currently being investigated in our laboratory by using human tumor xenografts as preclinical models of human cancer. The advantage of preclinical studies is that the experimental conditions can be controlled more easily than in clinical experiments. Furthermore, preclinical studies allow a range of experiments that is not possible in a clinical study. This makes it possible to compare detailed biological data with DCE-MRI

data. Several studies in our laboratory have investigated the potential of DCE-MRI in assessing the physiological microenvironment in tumors (Egeland et al., 2012; Gulliksrud et al., 2009; Vestvik et al., 2007). Our laboratory has especially focused on the potential that DCE-MRI might have in assessing hypoxia, and these studies have in most cases used intradermally implanted melanomas as tumor models (Egeland et al., 2008; Egeland et al., 2009; Egeland et al., 2012; Vestvik et al., 2007). In the current work, investigation of the potential of DCE-MRI as a biomarker for hypoxia was extended to include intramuscularly implanted melanomas. Additionally, the ability of DCE-MRI to predict response to fractionated radiation treatment was evaluated. Finally, emphasis was placed on the potential that DCE-MRI may have as a biomarker for metastatic disease.

The specific aims of the present work were:

To investigate the potential usefulness of DCE-MRI as a biomarker for:

- Hypoxia
- Response to radiation therapy
- Metastatic potential

LIST OF PUBLICATIONS

I. Ellingsen, C., Øvrebø, K.M., Galappathi, K., Mathiesen, B., and Rofstad, E.K. (2012). The pO_2 fluctuation pattern and cycling hypoxia in human cervical carcinoma and melanoma xenografts. Int. J. Radiat. Oncol. Biol. Phys. 83, 1317-1323.

II. Gulliksrud, K., Øvrebø, K.M., Mathiesen, B., Rofstad, E.K. (2011). Differentiation between hypoxic and non-hypoxic experimental tumors by dynamic contrast-enhanced magnetic resonance imaging. Radiother. Oncol. 98, 360-364.

III. Øvrebø, K.M., Hompland, T., Mathiesen, B., and Rofstad, E.K. (2012). Assessment of hypoxia and radiation response in intramuscular experimental tumors by dynamic contrast-enhanced magnetic resonance imaging. Radiother. Oncol. 102, 429-435.

IV. Øvrebø, K.M., Gulliksrud, K., Mathiesen, B., and Rofstad, E.K. (2011). Assessment of tumor responsiveness and metastatic potential by dynamic contrast-enhanced magnetic resonance imaging. Int. J. Radiat. Oncol. Biol. Phys. 81, 255-261.

V. Øvrebø, K.M., Ellingsen, C., Hompland, T., and Rofstad, E.K. (2012). Dynamic contrast-enhanced magnetic resonance imaging of the metastatic potential of tumors: A preclinical study of cervical carcinoma and melanoma xenografts. Acta Oncologica. doi:10.3109/0284186X.2012.689851

VI. Øvrebø, K.M., Ellingsen, C., Galappathi, K., and Rofstad E.K. (2012). Dynamic contrast-enhanced magnetic resonance imaging of the metastatic potential of human melanoma xenografts. Int. J. Radiat. Oncol. Biol. Phys. 83, e121-e127.

INTRODUCTION

Tumor physiology

Angiogenesis

Angiogenesis − the formation of new vessels − is governed in both normal and neoplastic tissue by the net balance between pro- and antiangiogenic factors (Carmeliet and Jain, 2000). For clusters of cells to grow beyond a certain size (1-2 mm in diameter), a vasculature is needed to provide nutrients and oxygen. Consequently, angiogenesis is one of the hallmarks of cancer, being a necessity for further growth of all solid tumors (Hanahan and Weinberg, 2000; Hanahan and Weinberg, 2011). The cellular aggregates may, however, enter a dormant phase for many years if the angiogenic process fails. Such dormant cellular aggregates are often referred to as tumor in situ and may remain dormant indefinitely (Folkman and Kalluri, 2004). The angiogenic switch can be turned on at any time, and when the angiogenesis is initiated, tumor growth, malignant progression, and metastatic dissemination may follow. In malignant tumors, the angiogenic process is out of control due to an imbalance between pro- and antiangiogenic factors, as illustrated in Figure 1b (Jain and Stylianopoulos, 2010). The balance between pro- and antiangiogenic factors is strictly controlled in normal tissue, and angiogenesis only occurs under special conditions such as embryonic development and wound healing. Pro- and antiangiogenic factors can originate from cancer cells, endothelial cells, stromal cells, blood, or the extracellular matrix (Carmeliet and Jain, 2000). Well-known proangiogenic factors include fibroblast growth factor (FGF), vascular endothelial growth factor (VEGF), interleukin 8 (IL-8), and platelet-derived growth factor (PDGF). Examples of antiangiogenic factors include thrombospondin, tumstatin, canstatin, endostatin, angiostatin, and interferon alpha/beta (Folkman and Kalluri, 2004).

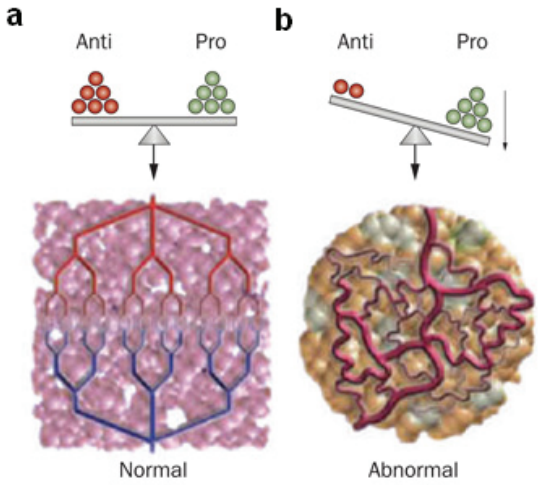

Figure 1: Angiogenesis is controlled by pro- and antiangiogenic factors. In tumors, there is an imbalance between pro- and antiangiogenic factors, causing an abnormal angiogenic process, which again leads to a chaotic vascular structure. a) Balance between pro- and antiangiogenic factors, resulting in a normal vasculature. b) Imbalance between pro- and the antiangiogenic factors, resulting in an abnormal vascular structure. The figure is reproduced from Jain and Stylianopoulos (2010).

In normal tissue, there are three different modes of vessel formation, whereas in neoplastic tissue there are six. These six modes of vessel formation are illustrated in Figure 2. The modes of vessel formation that can occur in normal tissue are:

- Sprouting angiogenesis; endothelial cells (ECs) in a preexisting blood vessel escape from the parent vessel wall into the surrounding matrix and form solid sprouts connecting neighboring vessels. Unlike all the other vessel formation mechanisms, sprouting angiogenesis creates entirely new vessels. (Fig. 2a)
- Vasculogenesis; angioblasts differentiate into ECs that assemble into a vascular labyrinth. (Fig. 2b)
- Intussusception; preexisting vessels split and give rise to new vessels. (Fig. 2c)

In tumors, the additional following modes of vessel formation may occur:

- Vessel co-option; tumor cells “hijack” the preexisting vasculature. (Fig. 2d)
- Vascular mimicry; tumor cells line existing vessels, mimicking ECs. (Fig. 2e)
- Tumor cell → EC differentiation; putative cancer stem-like cells create the tumor endothelium (Fig. 2f). This way of vessel formation is, however, much disputed.

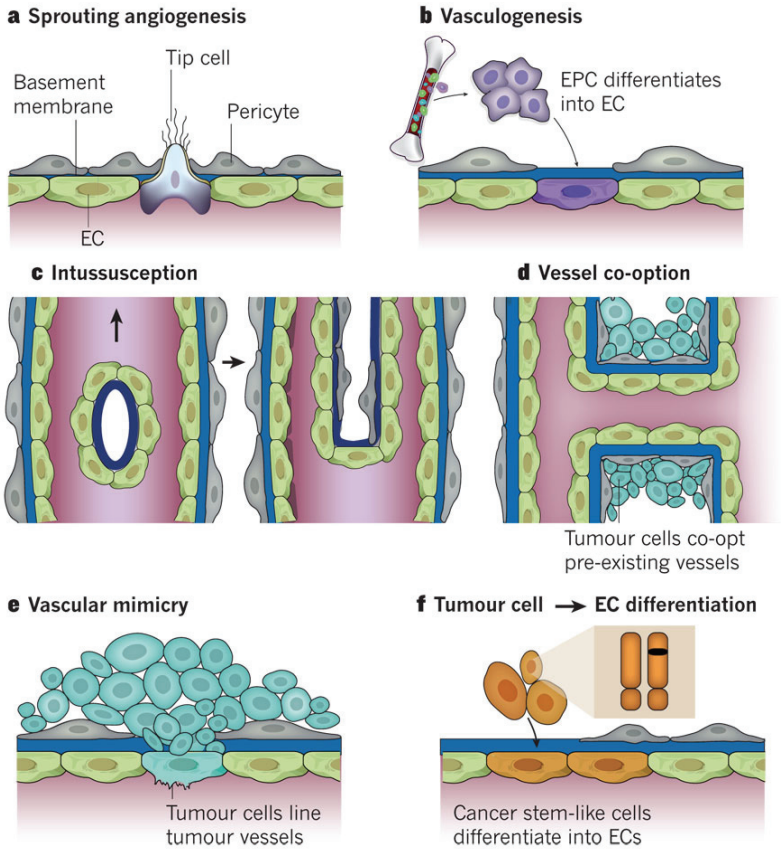

Figure 2: Modes of vessel formation. Sprouting angiogenesis a), vasculogenesis b), intussusception c), vessel co-option d), vascular mimicry e), cancer stem-like cells differentiate into ECs f). a-c can occur in both normal and neoplastic tissue, while d-f only occur in neoplastic tissue. The figure is reproduced from Carmeliet and Jain (2011).

Angiogenic activity is not necessarily correlated with tumor aggressiveness for all tumor types (Bergers and Benjamin, 2003). Nevertheless, the resulting abnormal vasculature may contribute to malignant progression and prevent chemotherapy from reaching the tumor cells (Jain, 2008). In 1971, Judah Folkman proposed that antiangiogenic drugs might be used to starve the tumor, thereby stopping the tumor's growth (Folkman, 1972). Since then, there has been an increased focus on antiangiogenic therapy, and today antiangiogenic drugs have been approved for clinical use for several types of cancer.

Vasculature and blood flow

The uncontrolled angiogenic process in tumors results in a disorganized tumor vasculature. Some of the differences between the vasculature in normal tissue and tumor tissue are shown in Figure 3. Unlike the vasculature in normal tissue, the vasculature in tumor tissue may lack a hierarchical structure and show severe architectural abnormalities. Tumor vessels are irregularly shaped, tortuous, elongated, dilated and may have dead ends (Bergers and Benjamin, 2003; Vaupel et al., 1989). They may share chaotic features from arterioles, capillaries and venules instead of being strictly defined (Bergers and Benjamin, 2003). Additionally, the microvascular density (MVD) within the tumor also differs to a larger degree than in normal tissue (Gillies et al., 1999).

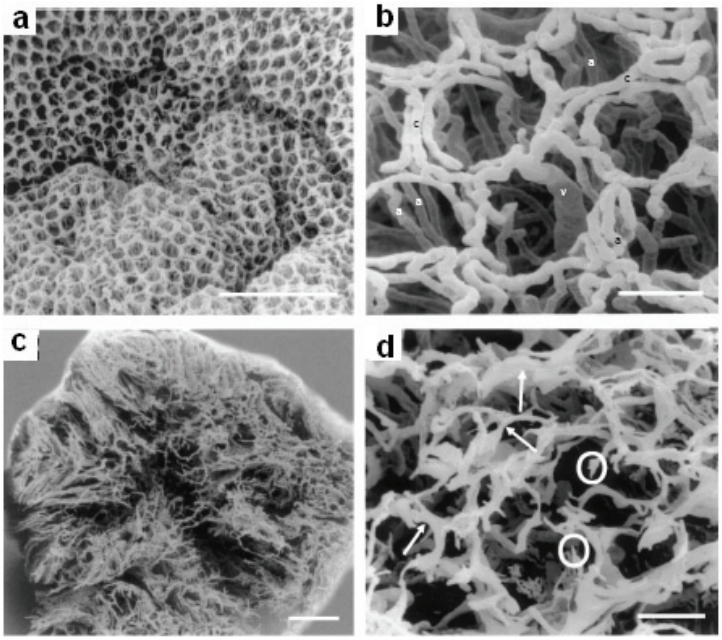

Figure 3: Images of the colorectal vasculature in normal mucosa a, b) and carcinoma c, d). In the normal mucosa, the vasculature is highly organized, whereas the vessels in the tumor are heterogeneously distributed, the vessel diameters vary (arrows), and there are dead ends (circles). The figure is reproduced from Konerding et al. (2001).

Moreover, the vessel walls in tumors may have incomplete or missing endothelial lining, interrupted or absent basement membrane, blood channels lined by tumor cell cords, and they may lack pericytes (Vaupel et al., 1989). As a result of these

abnormalities, tumor blood vessels may become more permeable than vessels in normal tissue. The vascular permeability can vary both within and among tumors (Tredan et al., 2007).

The abnormal morphology of the tumor vasculature combined with a decrease in vessel density may generate geometric resistance to blood flow, which in turn can lead to lower perfusion (Vaupel, 2004). The blood flow can be heterogeneous, with both highly perfused areas and areas that have little or no perfusion within the tumor (Vaupel et al., 1989). However, the variability in tumor blood flow seems to be greater *between* tumors than *within* a tumor (Vaupel, 2004). The low and heterogeneous blood perfusion in tumors may result in an inadequate supply of oxygen and nutrients in tumor regions.

Hypoxia

The oxygen level in cells is determined by the demand for and supply of oxygen to the cells (Gulledge and Dewhirst, 1996). The demand for oxygen by cells is determined by their cellular respiration. Moreover, the cell density in a specific area also has an impact on the total demand for oxygen in that area. The supply of oxygen is determined by the proximity of the cells to the vasculature, the amount of oxygen in the blood, and the blood flow. The demand for oxygen in tumors is not always met by the supply, resulting in tumor hypoxia. The demand for, and supply of, oxygen can vary within tumors, leading to heterogeneous oxygen levels within individual tumors (Wouters et al., 2002).

Generally, tumor hypoxia is divided into two categories based on the cause and/or duration of the low levels of oxygen. Chronic hypoxic cells are cells located outside the diffusion limit of oxygen, approximately 150 μm from a functional blood vessel. These cells are also referred to as diffusion-limited hypoxic cells. They will be chronically hypoxic since oxygen rarely reaches them through diffusion. Necrotic cells are often located next to chronically hypoxic cells. Acutely hypoxic cells are cells that are exposed to low levels of oxygen during a short period of time, often no more than a few minutes. These cells may, for instance, be located next to a transiently occluded vessel; acute hypoxia is, therefore, often referred to as transient hypoxia (Vaupel and Mayer, 2007). If the same tumor cells are repeatedly exposed to hypoxia, the term ‘cyclic hypoxia’ is often used about these acutely hypoxic cells. The two types of hypoxia are illustrated in Figure 4.

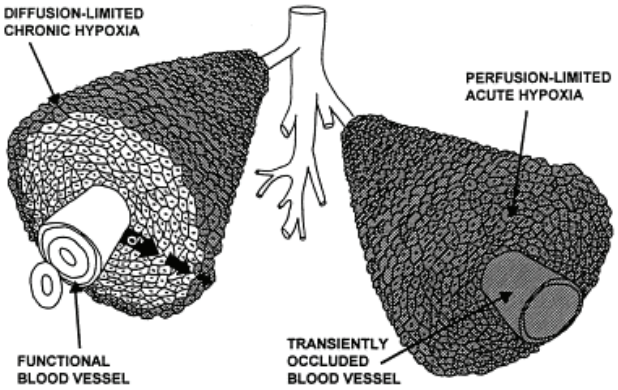

Figure 4: Schematic illustration of chronic and acute hypoxia. To the left: a functional blood vessel and chronic hypoxic cells located outside the diffusion limit of oxygen. To the right: a temporarily occluded blood vessel, hence acute hypoxia in the cells adjacent to the blood vessel. The figure is reproduced from Horsman (1998).

Normal oxygen levels vary in different organs; consequently, the threshold for hypoxia will vary from organ to organ (Vaupel, 1990). Nevertheless, radiosensitivity decreases rapidly for oxygen tensions (pO_2) lower than 10 mmHg, as illustrated in Figure 5. The oxygen tension of 10 mmHg is therefore often used as a threshold value for hypoxia. The biological damage produced by ionizing radiation comes from two different actions: direct and indirect, the latter of which demands oxygen in order to fully take effect. Direct action of radiation is seen when the radiation interacts directly with the DNA strand, while indirect action occurs when the radiation interacts with other atoms or molecules in the cell to produce free radicals. Free radicals can react with oxygen to create a peroxide form, which is a non-restorable form. The oxygen is thought to "fix" the damage so that it is irreparable. The indirect damage is responsible for approximately two thirds of the total damage when using X-rays, resulting in a diminished effect of the radiation where oxygen is lacking. The oxygen enhancement ratio (OER) is defined as the ratio of radiation doses under hypoxic to normoxic conditions required to obtain the same biological effect. For X-rays and gamma rays, the OER of high radiation doses has a value between 2.5 and 3.5 (Hall and Giaccia, 2006).

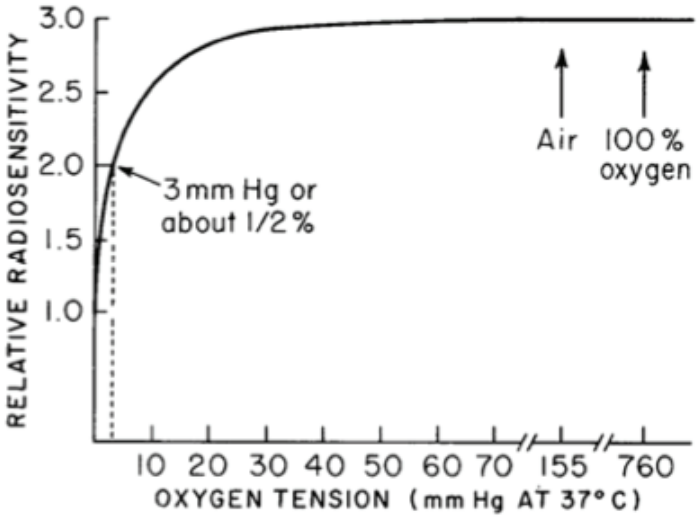

Figure 5: Idealized representation of the relationship between relative radiosensitivity and oxygen tension. The figure is reproduced from Hall and Giaccia (2006).

In addition, when the pO_2 levels are below 10 mmHg, cells increase their production of genes regulated by hypoxia inducible factor 1 (HIF-1) (Dewhirst et al., 2008). HIF-1 activation promotes the transcription of many genes that code for proteins involved in angiogenesis, glucose metabolism, cell proliferation, and metastasis (Semenza, 2003). Furthermore, overexpression of HIF-1α has been found in a wide range of human tumors and their metastases (Zhong et al., 1999). HIF-1 is an oxygen-sensitive transcriptional factor (Ke and Costa, 2006). Under hypoxic conditions, HIF-1α proteins translocate to the nucleus where they heterodimerize with HIF-1β proteins, forming the heterodimer HIF-1. Active HIF-1 then binds to distinct DNA sequences within hypoxia-response elements (HRE) and begins to transactivate specific target genes (Leo et al., 2004). Under normoxic conditions, HIF-1α is degraded (Ke and Costa, 2006).

Low levels of oxygen prevent cells from being killed by radiation; therefore, tumors with a significant amount of hypoxic cells are resistant to radiation therapy (Brown, 1999). Additionally, hypoxic cells in tumors are resistant to several anticancer drugs. This resistance is caused by various reasons, including the hindering of drug delivery and the hypoxic status affecting the toxicity of the drug (Brown and Wilson, 2004). Furthermore, a clinical study by Höckel et al. (1993) on patients with cancer of the uterine cervix has shown that patients with hypoxic tumors (Median $pO_2 \leq 10$ mmHg) have

a lower probability of both survival and recurrence-free survival than patients with non-hypoxic tumors, regardless of which standard treatment the patients are receiving. The probability of recurrence-free survival is shown in Figure 6 (Höckel et al., 1993). Similar results have also been presented for head and neck cancer and soft tissue sarcoma (Brizel et al., 1999; Nordsmark et al., 2001; Nordsmark and Overgaard, 2000).

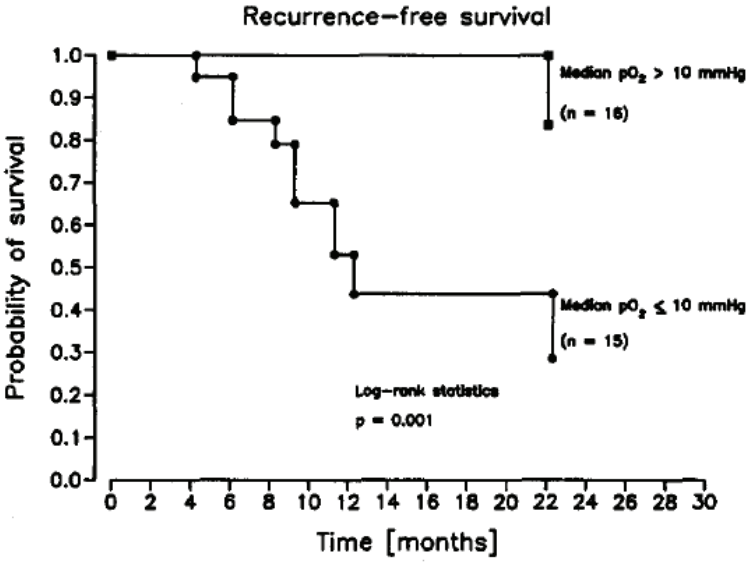

Figure 6: Probability of recurrence-free survival among patients with advanced cancer of the uterine cervix and median tumor pO_2 higher or lower than 10 mmHg. The median pO_2 level was determined prior to treatment by using Eppendorf probes. The figure is reproduced from Höckel et al. (1993).

There is a wide range of methods for determining the existence and/or extent of tumor hypoxia. These methods include radiobiological assays, pimonidazole experiments, oxygen electrodes, magnetic resonance imaging (MRI) techniques (e.g., blood-oxygen-level-dependent (BOLD) contrast), electron paramagnetic resonance (EPR), positron emission tomography (PET), and single photon emission spectroscopy (SPECT) (Hoogsteen et al., 2007; Horsman, 1998; Tatum et al., 2006; Vaupel and Mayer, 2007). There is currently no gold standard when it comes to measuring tumor hypoxia (Tatum et al., 2006). Every method has its advantages and limitations, and before attempting to measure hypoxia one should carefully consider the purpose of the measurement (Horsman, 1998).

Several strategies to combat hypoxia-related problems in cancer treatment have been suggested. These strategies include radiosensitizers, hyperthermic treatments, hyperbaric oxygen, nicotinamide and structurally related analogs, antiangiogenic drugs, accelerated fractionated radiotherapy combined with hyperoxic carbogen gas and nicotinamide (ARCON), bioreductive drugs, and gene therapy (Brown, 1999; Hoogsteen et al., 2007; Horsman, 1995; Wouters et al., 2002).

Interstitial fluid pressure

Most experimental and human tumors show increased interstitial fluid pressure (IFP) compared to normal tissue; measurements as high as 100 mmHg have been recorded in tumors (Heldin et al., 2004; Lunt et al., 2008). IFP is strictly controlled in normal tissue and is normally close to atmospheric levels (0 mmHg) (Lunt et al., 2008). The main driving force for elevated IFP in tumors is the hydrostatic microvascular pressure (MVP) (Boucher et al., 1990; Boucher and Jain, 1992). The abnormal vasculature in tumors results in increased geometric resistance to vascular blood flow, and the high vessel permeability in tumors allows fluid to flow easily from the vasculature into the interstitium. As a result, the MVP forces fluid from the vasculature into the tumor interstitium. In normal tissue, excessive fluid is drained away by the lymphatic system, but most tumors lack a functioning lymphatic system (Padera et al., 2002). Consequently, fluid accumulates in the interstitium, expands the elastic extracellular matrix, and causes interstitial hypertension (Milosevic et al., 1999).

Preclinical studies have shown that tumor IFP is uniform throughout the center of the tumor and decreases drastically at the rim of the tumor (Boucher et al., 1990; Rofstad et al., 2002b). A characteristic experimental tumor IFP profile is shown in Figure 7. Clinical studies, however, have suggested some spatial heterogeneity within central parts of the tumor (Milosevic et al., 1998).

IFP is a reflection of the global pathophysiology and may, therefore, have value as a biomarker for diagnosis and/or prognosis (Fukumura and Jain, 2007). Furthermore, there is no general correlation between tumor IFP and oxygenation, even though tumor IFP is inversely correlated to oxygenation in some tumors (Boucher et al., 1995). Several studies suggest that high IFP in the tumor is correlated with poor prognoses (Heldin et al., 2004). This has been seen in a study of patients with cervical cancer, where the recurrence rate was higher in patients with primary tumors with high IFP (Fyles et al., 2006). Furthermore, preclinical studies have suggested that elevated IFP is associated

with pulmonary and lymph node metastasis independent of hypoxia, and with poor radiocurability (Rofstad et al., 2002b; Rofstad et al., 2009; Rofstad et al., 2010b).

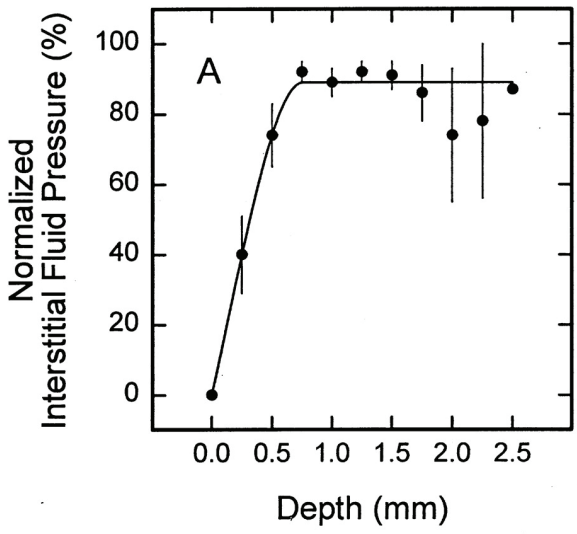

Figure 7: IFP profile of human melanoma xenografts. IFP is measured from the tumor rim. Individual points refer to the means of six tumors, and bars represent the standard error. The figure is reproduced from Rofstad et al. (2002b).

Elevated IFP in tumors can compromise the delivery of blood-borne therapeutic agents to tumors (Fukumura and Jain, 2007; Heldin et al., 2004; Lunt et al., 2008). Therapeutics move from the vasculature into the interstitium, either by diffusion or by convection (Lunt et al., 2008). Compounds with high molecular weight are mainly transported by convection, whereas compounds of lower molecular weight are transported by diffusion (Heldin et al., 2004; Lunt et al., 2008). High IFP in tumors limits or even eliminates the pressure gradient across the vessel wall, thus hindering the uptake of some cancer drugs. In addition, the pressure gradient in the periphery of the tumor may force drugs already in the interstitium out of the tumor.

Extracellular pH

Intracellular pH (pH_i) in tumors is neutral or alkaline, whereas extracellular pH (pH_e) is acidic. The result is a reversed pH gradient across the tumor-cell plasma membrane ($pH_i > pH_e$) in tumors compared to normal tissue, where pH_e is higher than pH_i (Stubbs et al., 2000). There are several reasons for low pH_e in tumors, one of them being

the altered glucose metabolism in tumors, which results in high lactic acid production. Another reason for the extracellular acidity is the increased level of carbonic acid. Insufficient drainage due to the lack of a functioning lymphatic system in tumors leads to an accumulation of protons, hence a lower pH_e (Fukumura and Jain, 2007; Vaupel, 2004). A preclinical study has shown that pH_e decreases with increasing distance from the nearest blood vessel, as presented in Figure 8. Additionally, the same study demonstrated that there is no general spatial correlation between low pH_e and hypoxia (Helmlinger et al., 1997).

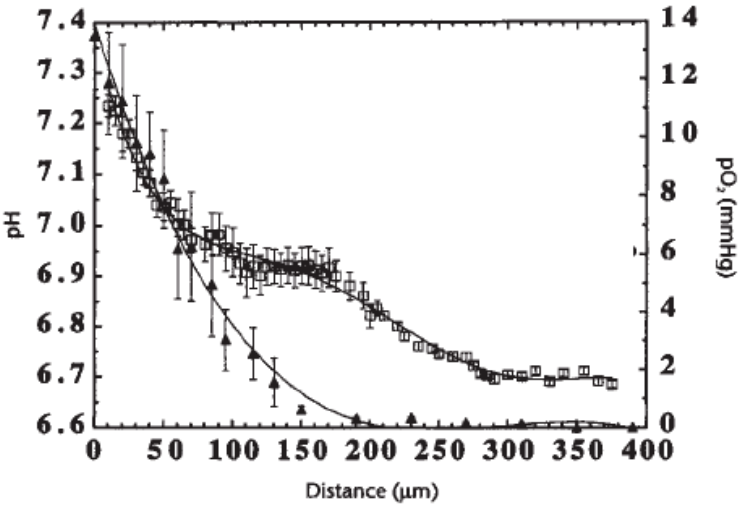

Figure 8: Mean interstitial pO_2 and mean extracellular pH as a function of distance from the nearest blood vessel. Open squares: pH_e. Closed triangles: pO_2. The figure is reproduced from Helmlinger et al. (1997).

Studies on human melanoma xenografts have suggested that acidic pH_e may increase the invasiveness and the angiogenic potential of tumor cells, and promote metastasis (Rofstad et al., 2006). In addition, clinical studies on human cervical carcinoma and head and neck tumors have shown that high lactate levels in the primary tumor are associated with a high risk of metastatic growth (Walenta et al., 1997; Walenta et al., 2000). Furthermore, acidic pH_e can affect the outcome of therapy because the reversed pH gradient in tumors hinders the uptake of basic drugs, and may increase the uptake of acidic drugs (Tredan et al., 2007).

Metastases

More than 90% of cancer-related deaths can be attributed to metastases (Wirtz et al., 2011). In order to establish distant metastases there are several steps in the metastatic process that have to be completed (Fidler, 1978; Steeg, 2006; Wirtz et al., 2011). Understanding the process leading to distant metastasis is, therefore, important. This chapter will give an overview of the metastatic process and the impact the physiological microenvironment of the primary tumor may have on the metastatic process.

The metastatic process

The most important and most common routes of metastatic dissemination involve dissemination by the blood vessels and/or lymphatics (Poste and Fidler, 1980). Among the tumor cells that reach the circulatory system, only 0.1% are able to survive and complete the metastatic process (Fidler et al., 1978). Lymph node metastasis and hematogenous metastasis can be driven by distinctly different mechanisms; however, several steps in the metastatic process are similar. An overview of the metastatic process is presented in Figure 9.

The process starts with the establishment and vascularization of the primary tumor. The vasculature provides the tumor with oxygen and nutrients, as well as facilitating the invasion of cancer cells into the blood vessels. Lymphangiogenesis may start simultaneously with the angiogenesis, and can be driven by some of the same growth factors (Cao, 2005; Wong and Hynes, 2006). Several studies have shown increased numbers of lymphatics surrounding growing tumors; however, the existence of a functioning lymphatic system within the tumor is debated (Cao, 2005; Wong and Hynes, 2006). In either case, the existence of both peritumoral and intratumoral lymphatics has been positively correlated with lymphatic metastasis (Cao, 2005).

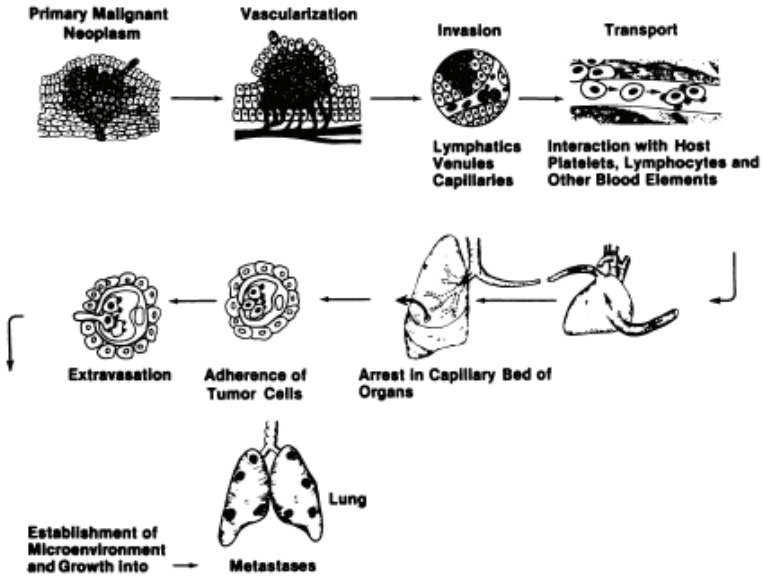

Figure 9: The metastatic process. In order to develop distant metastases, several steps have to be fulfilled. The figure is reproduced from Fidler (1978).

To be able to metastasize, cancer cells must detach from the primary tumor and invade blood vessels or lymphatics. The process of detachment and invasion can be either passive, where the cells are shed from the primary tumor, or active, by directed migration (Wong and Hynes, 2006). The transport of cancer cells is not necessarily carried out exclusively by the lymphatics or by the vasculature; cancer cells may begin to be disseminated in the lymphatics and then transported into the vasculature. During transport, the cancer cells may experience interactions, such as aggregation with other tumor cells, platelets, lymphocytes, and other host cells (Fidler, 1978). Furthermore, cancer cells transported by blood vessels can experience serum toxicity, high shear stresses, and mechanical deformation. Cancer cells traveling by the lymphatics have some advantages over those in the blood circulation because the smallest lymphatic vessels are larger than the blood capillaries, and the flow velocities in the lymphatics are orders of magnitude lower than those in the blood vessels. Furthermore, lymphatic vessels are filled with interstitial fluid, which promotes tumor cell viability (Pepper et al., 2003). Cancer cells traveling in clusters are more likely to establish metastasis than cells traveling alone. Additionally, it has been suggested that cancer cells bringing stromal components,

including fibroblasts, from the primary tumor, also increase their probability of successfully establishing distant metastases (Duda et al., 2010).

Cancer cells in the lymphatic system are first carried to the regional lymph nodes where they may proliferate; regional lymph nodes are therefore a common site for the initial spread of cancer. Cancer cells in the blood stream tend to be arrested in capillary beds, then penetrate the walls of these tiny vessels, and finally invade the surrounding tissue. Because of the blood-flow pattern, cancer cells usually meet their first capillary beds in the lungs; the lungs are thus a frequent site for metastases (Becker et al., 2006). The growth of a new tumor in a secondary organ is considered to be the most challenging step which cancer cells meet during the metastatic process (Chambers et al., 1995).

There are two different theories regarding which distant organ cancer cells in the circulatory system settle will in: the seed and soil hypothesis, and the anatomical/mechanical hypothesis. The seed and soil hypothesis was established in 1889 by Stephen Paget, who examined postmortem data from women with breast cancer and realized that the organ distribution of metastases in the patients was non-random. He suggested, therefore, that some tumor cells (the "seeds") prefer certain organs (the "soil") (Paget, 1989). The mechanical/anatomical theory postulates that it is the anatomy of the vasculature and lymphatic drainage from the site of the primary tumor that determines the pattern of the metastases. Today it is believed that the two theories are not mutually exclusive and that their influence depends on the primary tumor investigated (Langley and Fidler, 2011).

The tumor microenvironment and metastatic disease

The metastatic process is most likely not random since the cancer cell has to acquire a range of properties to be able to fulfill all the steps of the process (Woodhouse et al., 1997). Moreover, the microenvironment of the primary tumor may contribute to the regulation of cell phenotype, and might therefore have an impact on the malignant progression (Rofstad, 2000; Subarsky and Hill, 2003). Several studies, both clinical and preclinical, have shown that hypoxia, acute and chronic, affects the extent of metastasis (Brizel et al., 1996; Cairns et al., 2001; Rofstad et al., 2010a; Young et al., 1988). It has also been shown that pH_e influences the extent of metastasis (Jang and Hill, 1997; Rofstad et al., 2006). Fewer studies have evaluated the relationship between elevated IFP and metastasis; however, some studies have shown that elevated IFP increases the probability of metastasis (Milosevic et al., 2001; Rofstad et al., 2002b).

Acquisition of the necessary traits for a cell to metastasize may arise from the accumulation of specific mutations and/or transient changes in gene expression. These genes code for proteins which may be utilized by the cancer cell at different steps in the metastatic process. These steps include angiogenesis, invasion/migration, and survival (Subarsky and Hill, 2003). Examples of such proteins involved at different steps of the metastatic process are VEGF, which is involved in angiogenesis, and urokinase-type plasminogen activator receptor (uPAR), which is involved in invasion and migration. Both of these have been associated with hypoxia and increased metastatic efficiency in human melanoma xenografts (Rofstad et al., 2002a; Rofstad and Danielsen, 1999).

DCE-MRI

In DCE-MRI, a contrast agent (CA) is injected intravenously, and a series of MR images is recorded before and during uptake of the CA in the tissue so that the change in signal intensity with time can be recorded for each voxel (Yankeelov and Gore, 2009). Uptake of the CA in the tissue is determined by several physiological parameters such as blood flow, vessel wall permeability, surface area of the capillaries, cell density, and extracellular volume fraction (ECVF) (Taylor et al., 1999; Weinmann et al., 1984).

CAs used in MRI are designed to increase the difference in signal intensity between different tissues. CAs change the inherent proton density of the tissue and/or the relaxation rates and, consequently, the MR signal from the tissue. Most CAs are designed to alter the longitudinal (T_1) and/or transversal (T_2) relaxation times. CAs that decrease T_1 cause a signal intensity increase in T_1-weighted images; therefore, these agents are often referred to as positive relaxation agents. CAs decreasing T_2, on the other hand, are often called negative relaxation agents because the T_2 reduction results in a signal intensity decrease in a T_2-weighted image (Yankeelov and Gore, 2009). Techniques where T_2 weighting is used in DCE-MRI are often referred to as dynamic susceptibility contrast magnetic resonance imaging (DSC-MRI).

Gd-DTPA is one of the most commonly used CAs. It is a stable paramagnetic complex with a molecular weight of about 550 Da; it is distributed extracellularly, is rapidly excreted from the body, and is generally well tolerated (Weinmann et al., 1984). A paramagnetic CA such as Gd-DTPA increases the contrast between different tissues by decreasing T_1 and T_2. The magnitude of the effect of Gd-DTPA on the two different relaxation times is dependent on the concentration of Gd-DTPA. At low concentrations,

the T_1-relaxation-rate will be significantly more decreased than the T_2-relaxation-rate, whereas at high concentrations, mainly the T_2-relaxation-rate will be decreased (Hendrick and Haacke, 1993).

DCE-MRI data acquisition for quantitative analysis

To perform quantitative analysis of DCE-MRI data, three steps have to be taken during the DCE-MRI data acquisition. First of all, a method is needed to determine the concentration of the CA in the tissue. One method is T_1 mapping, which demands several T_1-weighted images taken at different flip angles. This method assumes a linear relationship between signal intensity increase and the concentration of the CA (Yankeelov and Gore, 2009). Another method is that used by Hittmair et al. (Hittmair et al., 1994). This method requires proton density images and the use of phantoms with known concentrations of the CA.

Secondly, several T_1-weighted images have to be taken before and after administration of the CA.

Thirdly, knowledge about the concentration of the CA in the arteries as a function of time, often referred to as the arterial input function (AIF), is necessary for almost all quantitative DCE-MRI data analysis (Yankeelov and Gore, 2009). There are several ways to measure the AIF; the methods either involve individual measurements or assume that the AIF is similar for all subjects. Individual measurements can be taken by obtaining the AIF from the DCE-MRI dataset by measuring the uptake in a large arterial vessel within the field of view of the DCE-MRI uptake, or by introducing an arterial catheter into the subject and sampling the blood during the measurements. The advantage of the first method is its noninvasiveness, while the disadvantage is the demand for a large arterial vessel within the image and the restrictions that this implies. Laboratory mice have a total blood volume of approximately 2 ml, so when working with them it is difficult to withdraw the required number of blood samples. By assuming a similar AIF for all subjects, it is only necessary to perform blood measurements on a cohort of subjects and then assume that the resulting average AIF is valid for subsequent studies. The advantage of using a common AIF is that no more AIF measurements are required during the DCE-MRI imaging. The method ignores any variation in the injection rate and differences in AIF between individuals (Yankeelov and Gore, 2009).

Quantitative analysis of DCE-MRI data

Quantitative analyses are based on fitting the DCE-MRI data to mathematical models. The most elementary quantitative model describes the body as one compartment; the CA enters the compartment with a volume V, at a specific rate constant k_a, and is eliminated with a rate constant k_e. Normally, CAs are distributed at different rates in different tissues, and these kinetics are, therefore, better described by a two-compartment model (Yankeelov and Gore, 2009). In a two-compartment model, such as the one shown in Figure 10, the blood plasma is considered as one compartment and the extravascular extracellular space (EES) as the other. The CA enters the capillary and either remains in the capillary or extravasates to the EES.

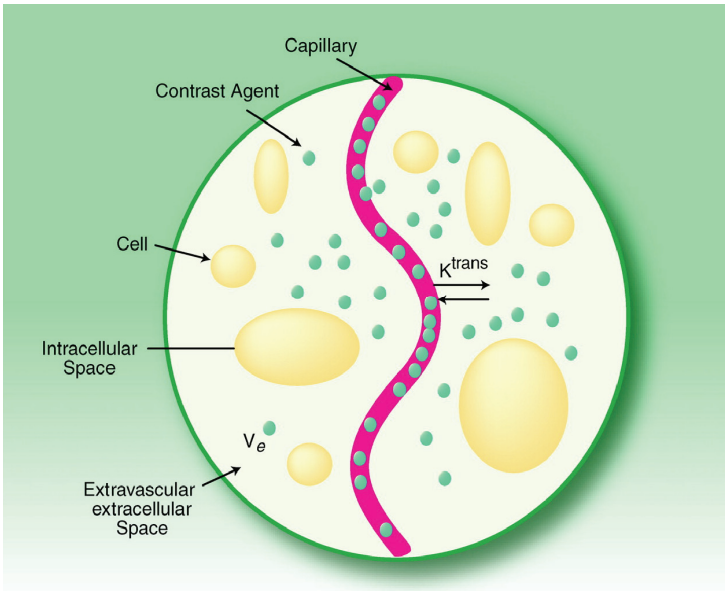

Figure 10: Illustration of the uptake of a CA in tissue. K^{trans} is the volume transfer constant of the CA. The CA does not enter the intracellular space; hence v_e is the extravascular extracellular volume fraction. The figure is reproduced from Jackson et al. (2007).

In 1999, several experts in the field of MR tracer kinetic models published a paper, in which they developed a generalized pharmacokinetic model, referred to as the generalized kinetic model of Tofts (Tofts et al., 1999):

$$C_t(T) = \frac{K^{trans}}{(1-Hct)} \cdot \int_0^T C_a(\tau) \cdot e^{-K^{trans} \cdot (T-\tau)/v_e} d\tau \qquad \textbf{Eq. 1}$$

where C_t (T) is the concentration of the CA in the tissue at time T after injection; K^{trans} is the transfer constant of the CA; Hct is the hematocrit; $C_a(\tau)$ is the concentration of the CA in the arteries at time τ ($C_a(\tau)$ is the arterial input function); and v_e is the extravascular extracellular volume fraction.

In addition to the assumption that the body consists of two compartments, the generalized kinetic model of Tofts also assumes that the CA is uniformly distributed in each compartment. Tofts' model is normally used as described in Eq. 1, with knowledge about the AIF and by calculating the CA-concentration from signal intensity, as for instance described by Hittmair et al. (1994). Another well-known two-compartment model is the Brix model, which most commonly does not make use of T_1 mapping, calculation of concentration from signal intensity (the use of phantoms), or AIF. This model is often used by calculating the relative signal intensity in each voxel, and not by calculating the concentration change in each voxel, which is common when one uses the model of Tofts.

Semiquantitative analyses and visual inspection

In addition to the quantitative approach to DCE-MRI, visual inspection and semiquantitative analyses can be carried out. Visual inspection is a subjective evaluation of the shapes of the time-signal intensity curves (Yankeelov and Gore, 2009). Semiquantitative analyses are less demanding than quantitative analysis, but are not as subjective as the methods where visual inspection is used. Parameters from semiquantitative analysis include the initial area under the curve (iAUC), the time to peak (TTP), and the slope of the washout curve. However, the physiological meaning of parameters derived from semiquantitative analysis is ambiguous. In addition, because semiquantitative analyses are based on signal intensity methods, the measurements can be influenced by scanner settings. Studies done at different times or at different institutions are therefore difficult to compare (Paldino and Barboriak, 2009; Yankeelov and Gore, 2009). The advantage of these methods, on the other hand, is that they are easily implemented, and several studies have successfully monitored cancer growth and treatment response by employing them (Yankeelov and Gore, 2009).

EXPERIMENTAL METHODS

The main methods used in this research are briefly summarized below. More detailed descriptions can be found in Papers I-VI.

Melanoma lines

Six human melanoma lines (A-07, C-10, D-12, R-18, U-25, V-27), grown either intradermally (i.d.) or intramuscularly (i.m.) in the legs of athymic mice, were used as tumor models for human melanomas. Two human cervix carcinoma lines (CK-160, TS-415), grown intramuscularly (i.m.), were used as tumor models of human cervix carcinomas. These tumor lines are permanent cell lines at our laboratory, and are described in detail elsewhere (Ellingsen et al., 2009; Rofstad, 1994; Rofstad and Mathiesen, 2010).

Tumor vasculature and connective tissue

Tumor microvasculature was studied by examining histological sections prepared from tumor tissue frozen in liquid nitrogen. The sections were immunostained for blood vessels or connective tissue by using a peroxidase-based indirect staining method. An anti-mouse CD31 rat monoclonal antibody (Research Diagnostics, Flanders NJ) or an anti-collagen rabbit polyclonal antibody (Dako, Glostrup, Denmark) was used as the primary antibody.

Tumor oxygen tension

Tissue pO_2 was measured simultaneously at two positions in each tumor using a fiber optic oxygen-sensing device (Oxylite 2000, Oxford Optronix, Oxford, U.K.). The pO_2 traces were subjected to detailed analysis. Thus, for each pO_2 trace, the fluctuation frequency (i.e., the number of pO_2 fluctuations per hour) around the mean pO_2 of the trace, and the amplitudes of the fluctuations were calculated by using the definitions and methods described elsewhere (Brurberg et al., 2004).

Irradiation

Tumors were irradiated in vivo under air-breathing or hypoxic conditions. An X-ray unit operated at 220 kV, 19-20 mA, and with 0.5-mm Cu filtration was used. The dose rate given to the xenografted tumors was 5.1 Gy/min.

Cell survival assay

Cell survival was measured in vitro using a plastic surface colony assay (Rofstad et al., 2007). Cells which gave rise to colonies >50 cells were scored as clonogenic. The cell-surviving fraction of a tumor given a single dose of irradiation was calculated from the plating efficiency of the cells of the irradiated tumors and the mean plating efficiency of six untreated control tumors. The cell-surviving fraction of a tumor given fractionated radiation treatment was corrected for the cell yields of the irradiated tumor and the six control tumors. In other words, the surviving fraction was measured relative to the number of clonogenic cells in the tumors right before the first radiation exposure (Rofstad, 1989).

Hypoxia

The fraction of radiobiological hypoxic cells (HF_{Rad}) was found by using the paired survival curve method, and the fraction of pimonidazole hypoxic cells (HF_{Pim}) was assessed in histological sections prepared from tumors fixed in phosphate-buffered 4% paraformaldehyde embedded in paraffin. The fractions of chronically hypoxic cells (HF_{Chr}) and acutely hypoxic cells (HF_{Acu}) were calculated from the fraction of radiobiological hypoxic cells (HF_{Rad}) and the fraction of pimonidazole-positive hypoxic cells (HF_{Pim}) as $HF_{Chr}=HF_{Pim}$ and $HF_{Acu}=HF_{Rad}-HF_{Chr}$ (Rofstad and Måseide, 1999).

Lymph node metastases

The mice were euthanized immediately after DCE-MRI and irradiation, and then examined for external lymph node metastasis in the inguinal, axillary, interscapular, and submandibular regions, and for internal lymph node metastases in the abdomen and mediastinum.

Pulmonary metastases

Microscopic pulmonary metastases were detected by histological examination. Resected lungs were fixed in phosphate-buffered 4% paraformaldehyde and embedded in

paraffin. Histological sections were cut from each lobe at 100-µm intervals and stained with hematoxylin and eosin. Groups of five or more tumor cells were scored as a metastasis.

DCE-MRI and kinetic modeling

DCE-MRI was performed on a clinical 1.5 T whole body scanner (Signa, General Electric, Milwaukee, WI, U.S.A.) with a cylindrical slotted tube resonator transceiver coil specially constructed for mice (Rofstad et al., 1994; Seierstad et al., 2007). The animals were put on an adapted cradle of Styrofoam before being inserted into the coil to prevent excessive heat loss. In addition, a thermostatically regulated heating pad was used to maintain the temperature of the animal at 37-38°C while scanning. Two calibration tubes were placed adjacent to the animal in the coil, one with 0.5 mmol/L Gd-DTPA (Schering, Berlin, Germany) in 0.9% saline and the other with 0.9% saline. Firstly, a sagittal scan was used to localize the tumor, and to decide the position of the single axial section through the tumor, which was used during the rest of the scanning. An image matrix of 256×128, a field of view of 8×4 cm^2, and one excitation were used.

T_2-weighted images were recorded by using a spin echo sequence with TR = 5000 ms and TE = 65 ms, followed by two proton density images (TR = 900 ms, TE = 3.2 ms, and $\alpha_{pd} = 20°$). Then three T_1-weighted images (TR = 200 ms, TE = 3.2 ms, and $\alpha_{T1} = 80°$) were recorded before Gd-DTPA was administered. The Gd-DTPA was diluted in 0.9% saline to a concentration of 0.06 M and administered into the tail vein of the mice in a bolus dose of 5.0 mL/kg (i.e., 0.3 mmol/kg), corresponding to an injection volume of 0.12-0.15 mL. The administration was performed manually during a period of 5 s by using a 24G-neoflon connected to a syringe by polyethylene tubing. Following the injection, T_1-weighted images were recorded for 15 minutes. The spatial resolution was 0.31×0.31×2.0 mm^3, and the time resolution was 14 s.

Using the method of Hittmair et al., the tissue concentrations of Gd-DTPA were calculated from the increase in signal intensities (Hittmair et al., 1994). The DCE-MRI series was then analyzed by using the arterial input function of Benjaminsen et al. (Benjaminsen et al., 2004) and the Tofts pharmacokinetic model (Tofts et al., 1999). The image analyses were performed using in-house developed software in IDL (Interactive Data Language). Parametric images of K^{trans} and v_e were generated with SigmaPlot software (SPSS Science, Chicago, IL, U.S.A.).

SYNOPSIS OF RESULTS

I. The pO_2 fluctuation pattern and cycling hypoxia in human cervical carcinoma and melanoma xenografts.

The purpose of this study was to investigate whether tumors of different histological types differ in pO_2 fluctuation pattern and extent of acute and chronic hypoxia. Cervical carcinomas CK-160 and TS-415, and melanomas A-07 and R-18 xenografts were included in the study. The microvasculature was investigated by histological examinations, and the results showed that the cervical carcinoma tumors had a higher fraction of connective tissue-associated blood vessels than the melanoma tumors. Furthermore, tissue pO_2 was measured in the tumors at two positions by using an Oxylite fiber optic oxygen-sensing device. In addition, the extent of acute and chronic hypoxia was assessed by combining a radiobiological and a pimonidazole-based immunohistochemical assay of tumor hypoxia. The temporal heterogeneity in tissue pO_2 was larger in the melanoma xenografts than in the cervical carcinoma xenografts. Moreover, the ratio of the fraction of acutely hypoxic cells to the fraction of chronically hypoxic cells (HF_{Acu}/HF_{Chr}) was higher in intradermal melanoma xenografts than in intramuscular cervical carcinoma xenografts.

II. Differentiation between hypoxic and non-hypoxic experimental tumors by dynamic contrast-enhanced magnetic resonance imaging.

To evaluate whether tumor hypoxia can be assessed by DCE-MRI, three tumor models without hypoxic tissue (small A-07 i.d., small A-07 i.m., and small R-18 i.d.) and three with hypoxic regions (large A-07 i.d., large A-07 i.m., and large R-18 i.d.) were subjected to DCE-MRI. The hypoxic statuses of the tumor models were determined by using a radiobiological assay and a pimonidazole-based immunohistochemical assay. Median K^{trans} was significantly higher in the non-hypoxic tumors; however, median v_e was not able to differentiate the hypoxic tumors from the non-hypoxic tumors. In addition, tumor response to fractionated radiation was measured by giving fractions of 2 Gy six times in 60 hours. The surviving fractions were significantly higher in the hypoxic tumors than in the non-hypoxic tumors.

III. Assessment of hypoxia and radiation response in intramuscular experimental tumors by dynamic contrast-enhanced magnetic resonance imaging.

Previous studies in our laboratory have suggested that DCE-MRI-derived parameters may provide valuable information about the extent of hypoxia in intradermal melanoma xenografts (Egeland et al., 2006; Egeland et al., 2008). In another previous study in our laboratory, it was shown that similar median K^{trans} and median v_e in intramuscular and intradermal tumors reflected different radiobiological hypoxic fractions (Gulliksrud et al., 2010). This study, therefore, investigated whether DCE-MRI has the potential for assessing the extent of tumor hypoxia in intramuscular melanoma xenografts. R-18, V-27, and U-25 intramuscular melanoma xenografts were subjected to DCE-MRI and then irradiated with a single dose of 10 Gy for determination of the radiobiological hypoxic fraction (HF_{Rad}). Median K^{trans} decreased with increasing HF_{Rad}, and the correlation was similar for the three tumor cell lines. Median v_e correlated with the surviving fraction after 10 Gy, but did not correlate with HF_{Rad}.

IV. Assessment of tumor responsiveness and metastatic potential by dynamic contrast-enhanced magnetic resonance imaging.

In this study we investigated whether DCE-MRI can be used to assess radiation resistance and metastatic potential. R-18 tumors grown intramuscularly were subjected to DCE-MRI followed by irradiation with either a single fraction of 10 Gy for detection of radiobiological hypoxia, or five fractions of 4 Gy in 48 hours to evaluate the radioresponsiveness. Finally, the host mice were euthanized before examination of lymph node metastases. Hypoxic tumors had lower median K^{trans} than non-hypoxic tumors. Furthermore, K^{trans} decreased with the increasing surviving fraction after fractionated radiation. Tumors in metastasis-positive mice had lower median K^{trans} than tumors in metastasis-negative mice. However, there was no significant correlation between median v_e and tumor hypoxia, radioresponsiveness, or metastatic potential.

V. Dynamic contrast-enhanced magnetic resonance imaging of the metastatic potential of tumors: A preclinical study of cervical carcinoma and melanoma xenografts.

To further investigate the potential of DCE-MRI for assessing metastatic potential, intramuscularly implanted CK-160 cervical carcinomas and V-27 melanoma tumors were used as tumor models. The tumors were first subjected to DCE-MRI; immediately afterwards, the host mice were euthanized before examination of lymph node metastasis. Highly metastatic tumors showed lower values for median K^{trans} than poorly metastatic tumors in both tumor models. Median v_e was lower for highly metastatic than for poorly metastatic V-27 tumors, but did not differ significantly for CK-160 tumors.

VI. Dynamic contrast-enhanced magnetic resonance imaging of the hypoxia-associated metastatic potential of human melanoma xenografts.

In Papers IV and V, the potential of DCE-MRI to provide information about the metastatic potential of tumors was investigated in intramuscular melanoma and cervical carcinoma xenografts which metastasized to the lymph nodes. In this study, we extended the analysis to intradermal melanoma xenografts and investigated the potential of DCE-MRI to provide biomarkers for hematogenous metastatic dissemination. C-10 and D-12 xenografts were subjected to DCE-MRI, followed by resection of the primary tumor and the lungs, which were prepared for histological assessment of the fraction of hypoxic cells and the presence of lung metastases. The primary tumors of the metastasis-positive mice had higher HF_{Pim} values, lower values of median K^{trans}, and lower values of v_e than the metastasis-negative mice.

DISCUSSION

Evaluation of methods

Relevance of tumor models

Human melanoma and cervix carcinoma xenografts grown intradermally (i.d.) or intramuscularly (i.m.) in athymic mice were used as models for human cancer in the current study. Cervical carcinoma xenografts were exclusively grown intramuscularly. Xenografted human tumors generally maintain many of the biological characteristics of the original human tumor (Sutherland et al., 1988). Studies of A-07, D-12, R-18, and U-25 tumors implanted orthotopically have shown that they retain the histological appearance, the microvessel density and ultrastructure, the angiogenic potential, the treatment response, and the organ-specific metastatic pattern of the original tumor (Rofstad, 1994). All melanoma cell lines used in this study mirror the aggressiveness of the donor patient's tumor when implanted orthotopically (Rofstad and Mathiesen, 2010). Examinations of the cervical carcinoma cell lines CK-160 and TS-145 have shown that, when they are grown intramuscularly, they have the same histological pattern, radiation sensitivity, and metastatic pattern of the original tumor (Ellingsen et al., 2009).

Several studies have suggested that animal models using orthotopically implanted tumors are more predictive of responses to therapeutics in the clinic than ectopically implanted tumors. Furthermore, orthotopic implantation is considered to be necessary for an accurate analysis of tumor growth and metastasis (Killion et al., 1998; Talmadge et al., 2007). However, studies where the same human cancer cell lines were implanted in different organs suggest that the vascularization and perfusion in the tumors will differ between the organs (Bernsen et al., 1999). Previous DCE-MRI studies in our laboratory have mainly been carried out on intradermal melanoma xenografts (Egeland et al., 2006; Egeland et al., 2008; Egeland et al., 2012). In the current study, we wanted to challenge the general validity of previous observations by studying intramuscular melanoma xenografts.

Paper I investigated whether the pO_2 fluctuation pattern and the extent of cycling hypoxia differ between tumor types showing high and low fractions of connective tissue-associated blood vessels. Two melanoma lines (A-07 and R-18) and two cervical

carcinoma lines (CK-160 and TS-415) were included in the study. These tumor models were selected for the study because the tumor microvessels in cervical carcinoma are located within broad bands of connective tissue, whereas microvessels in melanomas are not.

The main purpose of the study presented in Paper II was to investigate whether DCE-MRI has the potential to distinguish tumors with hypoxia from tumors without hypoxia. Six different tumor models were included in the study: small A-07 i.d., A-07 i.m., and R-18 i.d.; and large A-07 i.d., A-07 i.m., and R-18 i.d. tumors. The small tumors developed either no or an insignificant amount of tumor hypoxia, whereas all large tumors developed hypoxia. The development of tumor hypoxia depends on a range of factors such as the vascularity of the surrounding tissue, the potential of tumor cells to synthesize and secrete angiogenic factors, and the respiratory activity of the tumor cells and, hence, the cell density of the tumor tissue (Gillies et al., 1999; Gulledge and Dewhirst, 1996; Moulder and Rockwell, 1984). The chosen tumor models in Paper II show significant differences in cell density, secretion of IL-8 and VEGF A, and expression of PDGF and basic fibroblast growth factor (bFGF) (Egeland et al., 2009; Rofstad and Halsør, 2000; Vestvik et al., 2007).

Preliminary investigations have suggested that R-18, U-25, and V-27 are melanoma lines in which differences between intradermal and intramuscular tumors are particularly large. Intramuscularly injected R-18, U-25, and V-27 tumors were therefore chosen as tumor models in Paper III, since the main goal of the study was to investigate the potential of DCE-MRI in assessing tumor hypoxia in intramuscular melanoma xenografts.

Papers IV, V, and VI investigated whether low values of the DCE-MRI-derived parameters K^{trans} and v_e can be associated with metastatic potential. Tumor models included in these studies have all shown the ability to metastasize in previous studies in our laboratory (Ellingsen et al., 2009; Rofstad, 1994; Rofstad and Mathiesen, 2010). Furthermore, the metastatic potential is associated with hypoxia for some of the tumor models. Tumor hypoxia in R-18 (Paper IV) promotes lymph node metastasis by upregulating the expression of uPAR (Rofstad et al., 2002a). Tumor hypoxia in C-10 and D-12 (Paper VI), on the other hand, promotes lung metastases by upregulating the proangiogenic factors IL-8 and VEGF-A (Rofstad and Halsør, 2002; Rofstad and Mathiesen, 2010). Additionally, it has been shown that lymph node metastases in CK-160 (Paper V) tumors are associated with the fraction of hypoxic cells in the primary tumor

(Ellingsen et al., 2012). These tumor models are therefore particularly interesting for investigating the value that DCE-MRI has as a biomarker for metastatic potential, especially since it has been suggested that their metastatic efficiency is closely related to hypoxia.

It has been claimed that acutely hypoxic cells have higher metastatic potential than chronically hypoxic cells (Rofstad et al., 2007). The results from Paper I suggest that the temporal heterogeneity in tissue pO_2 and the fraction of hypoxic cells showing cycling hypoxia are larger in melanomas than in cervical carcinomas. In Paper V, cervical carcinoma CK-160 and melanoma V-27 tumors were used as tumor models. By including these models, it was possible to verify the validity of our DCE-MRI method both for tumors with a large degree of fluctuations in pO_2 and for tumors with a small degree.

Anesthesia and temperature effects

All experiments were carried out on anesthetized animals. An anesthetic consisting of fentanyl citrate, fluanisone, and midazolane was used. The use of this particular anesthetic may lead to a drop of 2-3°C in the body temperature if no precautions are taken. Such a drop in temperature is undesirable in this study as it may affect blood flow, consequently possibly affecting oxygenation. In order to avoid temperature drops in our experiments, heating pads and isolating materials were used. When maintaining the temperature, it has been verified that the anesthesia does not alter the tumor blood perfusion significantly (Gulliksrud et al., 2009).

Invasive measurements of tumor hypoxia

In the current study, three different invasive measurements of hypoxia were used: Oxylite probe measurements, the paired survival curve method, and immunohistochemistry with pimonidazole. The first method is the only one that determines oxygen partial pressure (pO_2), whereas the other two determine the fraction of hypoxic cells in a tumor.

Oxylite measurements

Oxylite measurements were used in Paper I to investigate whether fluctuation patterns differ among tumors of different histological types. The use of Oxylite measurements has some disadvantages. One of these is that measuring with probes makes it is difficult to know whether the measurements are taken in viable or necrotic tissue (Horsman, 1998). In order to avoid measurements in necrotic tissue in the current study,

the probes were positioned in tumor regions showing pO_2 values clearly higher than 0 mmHg. Another disadvantage of using the Oxylite system is that it provides poor spatial resolution; movements of the probes induce tissue trauma, which can influence the oxygen tension. Previous experiments in our laboratory have shown that, by excluding the first 20 minutes of the Oxylite measurements, artificially induced pO_2 fluctuations due to the insertion of the probes are avoided (Brurberg et al., 2005). Advantages of using Oxylite include high sensitivity in the hypoxic regions and excellent temporal resolution (Griffiths and Robinson, 1999).

Assessment of radiobiological hypoxic fraction (HF_{Rad})

The classic methods of estimating tumor hypoxia are based on radiation response. The three typical assays for assessing HF_{Rad} in animal systems are the paired survival curve method, tumor growth delay assay, and local tumor control assay (Horsman, 1998; Moulder and Rockwell, 1984). Of these three methods, the paired survival curve method is the most commonly used (Hall and Giaccia, 2006) and was indeed used in the current study.

There are both advantages and disadvantages to using a radiobiological assay for determining the fraction of hypoxic cells in a tumor. First of all, the fraction of radiobiological hypoxic cells is determined at the time the irradiation is given; therefore, radiobiological assays can not provide knowledge about the temporal kinetics associated with acute hypoxia. Secondly, information about the spatial distribution of the hypoxic cells in the tumor is lost in the paired survival curve method because the tumor is minced immediately after irradiation. However, when assessing the radiobiological hypoxic fraction, both chronic and acute hypoxia are detected (Fenton et al., 1995). Furthermore, the radiobiological hypoxic fraction is considered to be of greater clinical importance than hypoxic fractions derived from non-radiobiological assays, as only clonogenic cells are of relevance for tumor growth and response to treatment.

Assessment of pimonidazole-positive hypoxic fraction (HF_{Pim})

Pimonidazole can be used to detect various subpopulations of hypoxic cells. The concentration of pimonidazole injected, how it is injected, the time from injection to resection of the tumor, and the technique for producing the immunohistochemical preparations determine which subpopulation it measures (Gulliksrud et al., 2008). A pimonidazole assay which mainly measures chronically hypoxic cells has been

established in our laboratory (Rofstad and Måseide, 1999), and this assay was used in the current study.

Immunohistochemical assays do not distinguish between clonogenic and nonclonogenic cells. However, previous studies have shown a significant correlation between the radiobiological hypoxic fraction (HF_{Rad}) and the pimonidazole-positive hypoxic fraction (HF_{Pim}) in our melanoma xenografts (Egeland et al., 2012). Unlike radiobiological assays, this assay also provides spatial information about the hypoxic regions of the tumor (Fenton et al., 1995).

Calculating the fraction of acutely hypoxic cells from HF_{Rad} and HF_{Pim}

In the current study, we used the pimonidazole assay to measure chronically hypoxic cells; the fraction of chronically hypoxic cells (HF_{Chr}) is therefore equal to the fraction of pimonidazole-positive cells (HF_{Pim}). The fraction of acutely hypoxic cells could therefore be determined by the following equation: $HF_{Acu} = HF_{Rad} - HF_{Pim}$ (Rofstad and Måseide, 1999). Our definition of chronic and acute hypoxia is based on the assumption that the clonogeneity of chronically hypoxic cells is equal to the clonogeneity of the normoxic and acutely hypoxic cells. However, it has been suggested that the clonogeneity of chronically hypoxic cells is lower than that of normoxic cells (Fenton et al., 1995). Furthermore, this calculation assumes that the radiobiological hypoxic fraction and the immunohistochemical hypoxic fraction appear at the same oxygen tensions. This is not completely true, as immunohistochemical hypoxia appears at tensions below 10 mmHg, while 50% radiosensitivity occurs at pO_2 of 3.0 mmHg. In addition, it has been suggested that chronically hypoxic cells can be more sensitive to radiation than acutely hypoxic cells (Rofstad et al., 1999). Consequently, the fraction of acutely hypoxic cells may have been underestimated in this study (Paper I).

Radiation response assays

In Papers II and IV, the tumor response to fractionated radiation was measured in vitro using a clonogenic assay. The total dose of radiation was 12 Gy (6×2 Gy) in Paper II and 20 Gy (5×4 Gy) in Paper IV. It should be noted that clinically relevant treatment regimes would probably consist of approximately five and three times larger radiation doses, respectively. The use of a larger radiation dose than those employed in this study would probably result in a very low number of clonogenic cells and therefore lead to increased uncertainty. In addition, the clinical treatment regimes are given over a longer

period of time than in the studies reported herein. The surviving fractions were measured relative to the number of clonogenic cells in the tumors immediately before the first radiation exposure. Therefore, an extension of the treatment time would increase the uncertainty of the measurement. There are two other relevant assays that could have been considered instead of the cell survival assay. These are the tumor growth delay (TGD) and the tumor control (TCD_{50}) assays. Our experience with the TGD assay and large radiation doses is that the results have a higher uncertainty than those of the cell survival assay. In our study we wanted to look at individual tumors, and the tumor control assay (TCD_{50}) studies groups of animals, rather than individual tumors.

Detection of lymph node metastases

In the current study, the lymph node was scored as metastasis-positive when it was enlarged. Histological examinations previously performed in our laboratory have demonstrated that enlarged lymph nodes in melanoma xenografts contain metastatic deposits (Rofstad et al., 2002). There are, however, better methods for detecting lymph node metastases. One option could be to use cells transfected with green fluorescent protein (GFP); by doing so, the presence of micrometastases could be detected by studying the lymph nodes using a fluorescence microscope. This way, metastatic deposits which had not yet enlarged the lymph node would not be mistakenly characterized as metastasis-negative. However, a disadvantage is the possibility of detection of clusters of cells or even single cells that will not proliferate in the new location and establish a new tumor. By looking at enlarged lymph nodes, only cells that have grown in the new location are scored as metastasis positive.

Acquisition and analysis of DCE-MRI

MR-scanner and MR-coil

All MR-imaging in the current study was performed with a 1.5 T clinical whole body scanner. MR-imaging of the physiology in small tumors, such as the imaging performed in this study, is demanding, because high spatial resolution is necessary. In order to improve the signal to noise ratio (SNR), a small inductive coupled capacitive overlap transmit-receiver MR-coil specially designed for mice was used (Seierstad et al., 2007). The coil provides an adequate SNR for the spatial and temporal resolutions used in this study (Benjaminsen et al., 2004; Brurberg et al., 2007). An advantage of using a

clinical scanner is that it makes the possible transition from an animal MR procedure to a clinical MR procedure easier.

Limitations in the acquisition of the DCE-MRI series

Two significant limitations of the DCE-MRI study are the use of manual injection rather than the use of an infusion pump, and the use of a mean AIF instead of individual AIFs. Manual injection of a CA may lead to some variation among individuals; however, by using mean AIF, these variations are ignored. The mean AIF used in this study was determined previously by sampling blood from 12 mice and determining the concentration of Gd-DTPA by using MRI. Individual AIFs of three mice were compared to the mean AIF. The individual AIFs did not differ significantly from each other, or from the mean AIF (Benjaminsen et al., 2004). The mice used in this study have identical genetic backgrounds, which makes the use of a mean AIF valid. Moreover, the reproducibility of our DCE-MRI procedure was examined by imaging the same tumors twice within an interval of three hours. The resulting parametric images were found to be almost identical (Benjaminsen et al., 2004). The gain from using an infusion pump or individual AIFs would therefore probably be limited. Nevertheless, in a clinical setting, individual AIFs would be necessary due to the expected interpatient variability.

Furthermore, only one axial slice through the tumor was scanned in the DCE-MRI experiments. However, analysis of the results from a previous study in our laboratory, where a slice-interleaving acquisition method was used to cover the entire tumor, showed similar results in the parametric distribution from the entire tumor as for those derived from one axial slice (Gaustad et al., 2005). Therefore, it is unlikely that the results reported here would have been different if the entire tumor volume had been scanned instead of only one slice.

Correction for tumor necrosis

In the present study, the generalized kinetic model of Tofts was used to analyze the recorded DCE-MRI data. This model is based on material conservation and assumes equilibrium between the extracellular volume fraction (ECVF) and the blood. In necrotic tumor regions the assumption of equilibrium does not hold. The generalized kinetic model of Tofts is therefore not valid for necrotic tissue. Previous studies have demonstrated that, for all orthotopically implanted melanoma xenografts used in our laboratory, threshold values for v_e can be used to exclude voxels with nonphysiological v_e values (Egeland et al., 2012). Furthermore, significant correlations have been found

between the fraction of necrotic voxels assessed by our DCE-MRI method and the fraction of necrotic tissue assessed by histological examination (Egeland et al., 2008; Egeland et al., 2011). Consequently, voxels showing nonphysiological v_e values were excluded from the K^{trans} and v_e frequency distribution of the tumors. However, for the CK-160 tumors used in Paper V, it is not possible to differentiate between viable and necrotic tissue by using v_e with the spatial resolution that we have used. This is probably because the voxels consist of a mixture of different tissues (Ellingsen et al., 2010)

Observations in perspective

Assessment of tumor hypoxia by DCE-MRI

Tumor hypoxia results from an imbalance between the demand for and supply of oxygen (Gulledge and Dewhirst, 1996). Hypoxia is, therefore, expected to be found in regions with low blood perfusion and/or high cell density (i.e., low ECVF) (Jain, 1988; Vaupel, 1990). The DCE-MRI-derived parameters K^{trans} and v_e are assumed to represent blood perfusion and the extracellular volume fraction, respectively, in tumors showing high transvascular permeability to Gd-DTPA (Tofts et al., 1999). It has been established that, for our DCE-MRI procedure, these assumptions are valid for intradermally implanted A-07, D-12, R-18, and T-22 tumors (Egeland et al., 2009). It can therefore be hypothesized that low K^{trans} and/or v_e values would be a characteristic feature of hypoxic tumors.

The potential that K^{trans} and v_e may have in separating hypoxic from non-hypoxic tumors was investigated by using the following tumor models: A-07 i.d. (Paper II), R-18 i.d. (Paper II), A-07 i.m. (Paper II), and R-18 i.m. (Paper III). K^{trans} was significantly lower for hypoxic tumors than for non-hypoxic tumors for all the investigated tumor models. It was not possible, on the other hand, to make any distinction between hypoxic and non-hypoxic tumors with respect to v_e. Furthermore, the capability of our DCE-MRI method to determine the extent of tumor hypoxia was investigated in intramuscular R-18, U-25, and V-27 tumors (Paper III), and in intradermal C-10 and D-12 tumors (Paper VI). K^{trans} decreased with increasing hypoxic fraction for all the investigated tumor models. Additionally, v_e decreased with increasing hypoxic fraction for intradermal C-10 and D-12 tumors (Paper VI). The results confirm our expectations and are in accord with the hypothesis.

K^{trans} was related to the hypoxic status for all the tumor models used in the current study. This might imply that poor oxygen supply is the most important factor for hypoxia in the investigated tumor models. Additionally, v_e was related to hypoxia for intradermal C-10 and D-12 tumors (Paper VI), suggesting that, for these tumor models, the oxygen consumption also has a significant impact on the development of hypoxia in the tumor.

A study performed in our laboratory showed that K^{trans} and v_e decrease with increasing hypoxic fraction for eight different intradermal melanoma tumor models (Egeland et al., 2012). The results obtained in the current study are thus consistent with the study by Egeland et al. (2012). Furthermore, this study is an extension of the previous study because it includes intramuscularly implanted melanomas as well as intradermally implanted melanomas. Even though similar trends for K^{trans} and v_e have been shown for detecting the hypoxic fraction in intradermal and intramuscular tumors, it has been suggested that quantitative assessment of tumor hypoxia by DCE-MRI may require the use of tumor site-specific criteria when translating DCE-MRI data into hypoxic fractions (Gulliksrud et al., 2010).

Several clinical studies have also suggested that valid information about the hypoxic status may be obtained by using DCE-MRI. Cooper et al. (2000) used Eppendorf probes to measure tumor oxygenation in 30 patients with cervical carcinoma; DCE-MRI was performed prior to obtaining oxygenation data. Tumor oxygenation levels were found to correlate with their semiquantitative DCE-MRI-derived parameters (Cooper et al., 2000). Loncaster et al. (2002) also investigated the relationship between hypoxia and DCE-MRI-derived parameters for patients with carcinoma of the cervix. The study also used Eppendorf probes to measure tumor oxygenation; however, it used a pharmacokinetic model, the Brix model, and a semiquantitative analysis of the DCE-MRI data. Both semiquantitative and quantitative parameters correlated with tumor oxygenation. Newbold et al. (2009) examined whether there was a relationship between DCE-MRI-derived parameters and intratumoral hypoxia in seven patients with head and neck cancer. In that study, pimonidazole and CA9 staining were used as markers for hypoxia. Also in that study, they chose to analyze the data both semiquantitatively and quantitatively. Quantitatively, their analyses were performed by using a model similar to that of Tofts'. Their K^{trans} and v_e both correlated with hypoxia. However, contrary to our results, K^{trans} in that study increased with increasing degree of hypoxia. This can be explained by the fact that their K^{trans} values represent the leakiness of the vessels in the tumors, whereas K^{trans} for our tumor models represents blood perfusion. v_e, on the other

hand, as in our study, decreased with increasing degree of hypoxia and represented EES (Newbold et al., 2009). As in our study, these clinical studies have shown correlations between hypoxia in tumors and DCE-MRI-derived data. Taken together, these studies strongly suggest that DCE-MRI may be a useful method for identifying tumors with poor oxygenation.

Assessment of radiation response by DCE-MRI

Radiation resistance in tumors is closely related to hypoxia, and the current study has shown that DCE-MRI can be a valuable tool for detecting hypoxia in tumors. The potential that K^{trans} and v_e might have as predictive markers for response to fractionated radiation was therefore investigated for intradermal A-07 and R-18 tumors (Paper II), and intramuscular A-07 (Paper II) and R-18 (Paper IV) tumors. These studies showed that K^{trans} decreased with increasing surviving fraction. These results suggest that DCE-MRI has potential as a predictive tool for the outcome of fractionated radiation.

This suggestion is in agreement with several clinical studies (Zahra et al., 2007). Loncaster et al. (2002) had 50 cervical carcinoma patients that underwent DCE-MRI before being given radiotherapy. Their DCE-MRI data were analyzed both semiquantitatively and quantitatively; only one of the pharmacokinetic parameters (amplitude (A)) showed a statistically significant correlation with disease-specific survival (Loncaster et al., 2002). Semple et al. (2009) investigated whether DCE-MRI could predict outcome for patients with locally advanced cervical carcinoma treated with chemoradiation. Interestingly, they found a correlation between K^{trans} and clinical response (Semple et al., 2009). Yuh et al. (2009) investigated whether they could use DCE-MRI to predict control of the primary tumor and survival for patients with cervical cancer. They performed DCE-MRI before and twice during the radiation therapy course. The results from the DCE-MRI taken before treatment showed no correlation with control of the primary tumor or disease-free survival; however, there were some statistically significant correlations for the DCE-MRI-derived parameters from the DCE-MRI recordings during the course of treatment and control of the primary tumor and disease-free survival. Their data were analyzed semiquantitatively (Yuh et al., 2009). Zahra et al. (2009) analyzed data from just 13 patients with cervical cancer and found a correlation between both semiquantitatively derived parameters and quantitatively derived parameters, and tumor regression after radiotherapy. The most interesting result in that study was probably the correlation found between K^{trans} and tumor regression (Zahra,

2009). Semple et al. (2009) and Zahra et al. (2009) found that K^{trans} increased with increased response to treatment, which is consistent with our results. Direct comparisons of our results to those found in studies with semiquantitative analyses, are difficult because these parameters often have other physiological meanings than ours, or even an unclear physiological meaning. Furthermore, the correlations found in some of these clinical studies are also often generally weak; possibly the analysis was semiquantitative. Nevertheless, these studies do show a correlation between DCE-MRI-derived parameters and the outcome of radiotherapy. Consequently, this preclinical study can be seen as an extension of the existing clinical studies, and it warrants further clinical investigation. We will, however, based on the results of our study, recommend the use of pharmacokinetic models where K^{trans} and v_e are the derived parameters.

Assessment of metastatic potential by DCE-MRI

It has been demonstrated that hypoxia can promote metastasis (Brizel et al., 1996; Cairns et al., 2001; Rofstad et al., 2010a; Young et al., 1988). Furthermore, it has been suggested that cyclic hypoxia might be more important for the promotion of metastasis than chronic hypoxia (Dewhirst 2009; Rofstad, 2000). In the current work, we have shown that K^{trans} and v_e can give valuable information about the hypoxic fraction in the primary tumor. We therefore hypothesized that DCE-MRI would show promise as a biomarker for metastatic potential for tumors, in which hypoxia promotes the metastatic disease. We have shown that intramuscular R-18 (Paper IV), V-27 (Paper V), CK-160 (Paper V), and intradermal C-10 (Paper VI) and D-12 (Paper VI) tumors in metastasis-positive mice have significantly lower K^{trans} values than tumors in metastasis-negative mice. Furthermore, intradermal C-10 and D-12 tumors (Paper VI) in metastasis-positive mice have a significantly lower v_e than those in metastasis-negative mice. The results meet the expectation of the hypothesis.

In Paper V, CK-160 cervical carcinoma and V-27 melanoma xenografts were used as tumor models to investigate the potential that DCE-MRI might have in distinguishing between poorly and highly metastatic tumors. It has been shown that melanoma xenografts exhibit more cyclic hypoxia than do cervical carcinoma xenografts (Paper I). The DCE-MRI results from Paper V suggest that our DCE-MRI method works equally well for tumors with a lot of cyclic hypoxia, as for tumors with little cyclic hypoxia.

The draining lymphatics were investigated in Paper V, where it was discovered that they were enlarged in animals showing metastasis-positive inguinal lymph nodes.

This suggests that tumor hypoxia promotes lymphogenous metastatic spread by upregulating pro-lymphangiogenic factors. Several studies of different tumor types have shown correlations between tumor hypoxia, expression of the pro-lymphangiogenic factor vascular endothelial growth factor C (VEGF-C), lymphangiogenesis, and lymph node metastasis (Chaudary et al., 2011; Min et al., 2011; Schoppmann et al., 2006).

To our knowledge, there is only one other preclinical study so far which has investigated the usefulness of DCE-MRI as a biomarker for metastatic potential. The study, done by Li et al. (2007), used xenografted tumors of two melanoma lines transplanted subcutaneously into athymic mice. The tumors were subjected to gadodiamide-based DCE-MRI. It was shown that K^{trans} was significantly lower in the most metastatic line (C8161) compared to the least metastatic line (A375P). This result was consistent with the histological observation showing that the density of functional blood vessels was higher in the least metastatic line than in the most metastatic line. However, only three tumors of the most metastatic line and four of the least metastatic line were included. Also, the metastatic potential was based on historical information rather than on the metastatic status of the host. In addition, the differences in K^{trans} between the two lines were limited to the core of the tumors, and it was necessary to analyze the DCE-MRI data by the fast exchange regime-permitted model, a pharmacokinetic model incorporating the effects of transcytolemmal water exchange. Nevertheless, it was concluded that DCE-MRI may provide potential biomarkers for the metastatic potential in tumors (Li et al., 2007). This is strongly supported by the present study. Furthermore, in the current study, a large number of tumors was used. In addition, the differences in K^{trans} and v_e were found for the center as well as for the rim of the tumor, and the metastatic status of the tumor host was used to determine metastatic potential. Moreover, the analysis of the DCE-MRI data was performed by a relatively simple pharmacokinetic model, which has been recommended by both the US National Cancer Institute and the Pharmacokinetic Technologies Advisory Committee of Cancer Research UK for analysis of DCE-MRI data in clinical trials of anticancer therapeutics affecting tumor vascularization (Leach et al., 2003).

Several clinical studies have investigated the potential that DCE-MRI may have in predicting lymph node status, recurrence, or metastasis for breast cancer patients. Bahri et al. (2008) analyzed DCE-MRI data from 62 patients both semiquantitatively and pharmacokinetically by using the Tofts model. They found significant correlations between DCE-MRI-derived parameters and lymph node status at the time of the DCE-

MRI recording, and between the DCE-MRI parameters and recurrence after approximately five years (Bahri et al., 2008). Hsiang et al. (2007) recorded DCE-MRI data from 46 patients with locally advanced breast cancer receiving neoadjuvant chemotherapy. After the chemotherapy, the patients underwent mastectomy and lumpectomy, and axillary lymph node dissection. It was shown that the result from DCE-MRI can be predictive of the axillary nodal status after neoadjuvant chemotherapy (Hsiang et al., 2007). Loiselle et al. (2011) analyzed their DCE-MRI data from 167 patients semiquantitatively and found a significant difference in peak enhancement between patients who were lymph node positive and patients who were lymph node negative (Loiselle et al., 2011). Tuncbilek et al. (2011) investigated the relationship between DCE-MRI semiquantitative parameters and recurrence or metastasis for 49 patients with breast cancer. Two of the DCE-MRI parameters (maximal enhancement ratio within the first minute ($E_{max/1}$) and steepest slope) showed a statistically significant difference between patients with regard to recurrence or metastases (Tuncbilek et al., 2011). These studies differ in the choice of analysis method of the DCE-MRI data by using either semiquantitative or quantitative analysis of the DCE-MRI data. Nevertheless, all the studies have concluded that DCE-MRI-derived parameters from the primary tumor can be used as a predictive marker of lymph node status, metastasis, or recurrence for breast cancer patients. Together with the present preclinical study, this calls for further clinical investigations of the potential that DCE-MRI may have as a biomarker for metastatic potential.

CONCLUSIONS

Gd-DTPA-based DCE-MRI has been shown to provide valuable information about the existence as well as the extent of hypoxia in tumors.

The tumor response to radiation therapy may be predicted by the use of Gd-DTPA-based DCE-MRI.

Reliable information about metastatic potential can be obtained by Gd-DTPA-based DCE-MRI.

This preclinical study has used a well-known pharmacokinetic model in order to analyze the recorded DCE-MRI data. The results show convincing and statistically strong correlations with hypoxia, radiation response, and metastatic potential. We will therefore recommend the use of pharmacokinetic models in future clinical studies.

REFERENCES

Bahri, S., Chen, J-H., Yu, H.J., Kuzucan, A., Nalcioglu, O., and Su, M-Y. (2008). Can dynamic contrast-enhanced MRI (DCE-MRI) predict tumor recurrence and lymph node status in patients with breast cancer? Ann. Oncol. 19, 822-824.

Becker, W.M., Kleinsmith, L.J., and Hardin, J. (2006). The World of the Cell. Benjamin Cummings, San Francisco. 6th ed.

Benjaminsen, I.C., Graff, B.A., Brurberg, K.G., and Rofstad, E.K. (2004). Assessment of tumor blood perfusion by high-resolution dynamic contrast-enhanced MRI: a preclinical study of human melanoma xenografts. Magn. Reson. Med. 52, 269-276.

Bergers, G. and Benjamin, L.E. (2003). Tumorigenesis and the angiogenic switch. Nat. Rev. Cancer 3, 401-410.

Bernsen, H.J., Rijken, P.F., Hagemeier, N.E., and van der Kogel, A.J. (1999). A quantitative analysis of vascularization and perfusion of human glioma xenografts at different implantation sites. Microvasc. Res. 57, 244-257.

Boucher, Y., Baxter, L.T., and Jain, R.K. (1990). Interstitial pressure gradients in tissue-isolated and subcutaneous tumors: implications for therapy. Cancer Res. 50, 4478-4484.

Boucher, Y. and Jain, R.K. (1992). Microvascular pressure is the principal driving force for interstitial hypertension in solid tumors: implications for vascular collapse. Cancer Res. 52, 5110-5114.

Boucher, Y., Lee, I., and Jain, R.K. (1995). Lack of general correlation between interstitial fluid pressure and oxygen partial pressure in solid tumors. Microvasc. Res. 50, 175-182.

Brizel, D.M., Dodge, R.K., Clough, R.W., and Dewhirst, M.W. (1999). Oxygenation of head and neck cancer: changes during radiotherapy and impact on treatment outcome. Radiother. Oncol. 53, 113-117.

Brizel, D.M., Scully, S.P., Harrelson, J.M., Layfield, L.J., Bean, J.M., Prosnitz, L.R., and Dewhirst, M.W. (1996). Tumor oxygenation predicts for the likelihood of distant metastases in human soft tissue sarcoma. Cancer Res. 56, 941-943.

Brown, J.M. (1999). The hypoxic cell: A target for selective cancer therapy-- Eighteenth Bruce F. Cain Memorial Award Lecture. Cancer Res. 59, 5863-5870.

Brown, J.M. and Wilson, W.R. (2004). Exploiting tumour hypoxia in cancer treatment. Nat. Rev. Cancer 4, 437-447.

Brurberg, K.G., Benjaminsen, I.C., Dørum, L.M., and Rofstad, E.K. (2007). Fluctuations in tumor blood perfusion assessed by dynamic contrast-enhanced MRI. Magn. Reson. Med. 58, 473-481.

Brurberg, K.G., Graff, B.A., Olsen, D.R., and Rofstad, E.K. (2004). Tumor-line specific pO_2 fluctuations in human melanoma xenografts. Int. J. Radiat. Oncol. Biol. Phys. 58, 403-409.

Brurberg, K.G., Skogmo, H.K., Graff, B.A., Olsen, D.R., and Rofstad, E.K. (2005). Fluctuations in pO_2 in poorly and well-oxygenated spontaneous canine tumors before and during fractionated radiation therapy. Radiother. Oncol. 77, 220-226.

Cairns, R.A., Kalliomaki, T., and Hill, R.P. (2001). Acute (cyclic) hypoxia enhances spontaneous metastasis of KHT murine tumors. Cancer Res. 61, 8903-8908.

Cao, Y. (2005). Opinion: emerging mechanisms of tumour lymphangiogenesis and lymphatic metastasis. Nat. Rev. Cancer 5, 735-743.

Carmeliet, P. and Jain, R.K. (2000). Angiogenesis in cancer and other diseases. Nature 407, 249-257.

Carmeliet, P. and Jain, R.K. (2011). Molecular mechanisms and clinical applications of angiogenesis. Nature 473, 298-307.

Chambers, A.F., MacDonald, I.C., Schmidt, E.E., Koop, S., Morris, V.L., Khokha, R., and Groom, A.C. (1995). Steps in tumor metastasis: new concepts from intravital videomicroscopy. Cancer Metastasis Rev. 14, 279-301.

Chaudary, N., Milosevic, M., and Hill, R.P. (2011). Suppression of vascular endothelial growth factor receptor 3 (VEGFR3) and vascular endothelial growth factor C (VEGFC) inhibits hypoxia-induced lymph node metastases in cervix cancer. Gynecol. Oncol. 123, 393-400.

Cooper, R.A., Carrington, B.M., Loncaster, J.A., Todd, S.M., Davidson, S.E., Logue, J.P., Luthra, A.D., Jones, A.P., Stratford, I., Hunter, R.D., and West, C.M. (2000). Tumour oxygenation levels correlate with dynamic contrast-enhanced magnetic resonance imaging parameters in carcinoma of the cervix. Radiother. Oncol. 57, 53-59.

Dewhirst, M.W. (2009). Relationships between cycling hypoxia, HIF-1, angiogenesis and oxidative stress. Radiat. Res. 172, 653-665.

Dewhirst, M.W., Cao, Y., and Moeller, B. (2008). Cycling hypoxia and free radicals regulate angiogenesis and radiotherapy response. Nat. Rev. Cancer 8, 425-437.

Duda, D.G., Duyverman, A.M., Kohno, M., Snuderl, M., Steller, E.J., Fukumura, D., and Jain, R.K. (2010). Malignant cells facilitate lung metastasis by bringing their own soil. Proc. Natl. Acad. Sci. U.S.A. 107, 21677-21682.

Egeland, T.A., Gaustad, J.V., Benjaminsen, I.C., Hedalen, K., Mathiesen, B., and Rofstad, E.K. (2008). Assessment of fraction of hypoxic cells in human tumor xenografts with necrotic regions by dynamic contrast-enhanced MRI. Radiat. Res. 169, 689-699.

Egeland, T.A., Gaustad, J.V., Galappathi, K., and Rofstad, E.K. (2011). Magnetic resonance imaging of tumor necrosis. Acta Oncol. 50, 427-434.

Egeland, T.A., Gaustad, J.V., Vestvik, I.K., Benjaminsen, I.C., Mathiesen, B., and Rofstad, E.K. (2006). Assessment of fraction of radiobiologically hypoxic cells in human melanoma xenografts by dynamic contrast-enhanced MRI. Magn. Reson. Med. 55, 874-882.

Egeland, T.A., Gulliksrud, K., Gaustad, J.V., Mathiesen, B., and Rofstad, E.K. (2012). Dynamic contrast-enhanced-MRI of tumor hypoxia. Magn. Reson. Med. 67, 519-530.

Egeland, T.A., Simonsen, T.G., Gaustad, J.V., Gulliksrud, K., Ellingsen, C., and Rofstad, E.K. (2009). Dynamic contrast-enhanced magnetic resonance imaging of tumors: preclinical validation of parametric images. Radiat. Res. 172, 339-347.

Ellingsen, C., Egeland, T.A., Galappathi, K., and Rofstad, E.K. (2010). Dynamic contrast-enhanced magnetic resonance imaging of human cervical carcinoma xenografts: Pharmacokinetic analysis and correlation to tumor histomorphology. Radiother. Oncol. 97, 217-224.

Ellingsen, C., Hompland, T., Mathiesen, B., and Rofstad, E.K. (2012). Microenvironment-associated lymph node metastasis of human cervical carcinoma xenografts. Acta Oncol. 51, 465-472.

Ellingsen, C., Natvig, I., Gaustad, J.V., Gulliksrud, K., Egeland, T.A., and Rofstad, E.K. (2009). Human cervical carcinoma xenograft models for studies of the physiological microenvironment of tumors. J. Cancer Res. Clin. Oncol. 135, 1177-1184.

Fenton, B.M., Kiani, M.F., and Siemann, D.W. (1995). Should direct measurements of tumor oxygenation relate to the radiobiological hypoxic fraction of a tumor? Int. J. Radiat. Oncol. Biol. Phys. 33, 365-373.

Fidler, I.J. (1978). Tumor heterogeneity and the biology of cancer invasion and metastasis. Cancer Res. 38, 2651-2660.

Fidler, I.J., Gersten, D.M., and Hart, I.R. (1978). The biology of cancer invasion and metastasis. Adv. Cancer Res. 28, 149-250.

Folkman, J. (1972). Anti-angiogenesis: new concept for therapy of solid tumors. Ann. Surg. 175, 409-416.

Folkman, J. and Kalluri, R. (2004). Cancer without disease. Nature 427, 787.

Fukumura, D. and Jain, R.K. (2007). Tumor microenvironment abnormalities: causes, consequences, and strategies to normalize. J. Cell Biochem. 101, 937-949.

Fyles, A., Milosevic, M., Pintilie, M., Syed, A., Levin, W., Manchul, L., and Hill, R.P. (2006). Long-term performance of interstitial fluid pressure and hypoxia as prognostic factors in cervix cancer. Radiother. Oncol. 80, 132-137.

Gaustad, J.V., Benjaminsen, I.C., Graff, B.A., Brurberg, K.G., Ruud, E.B., and Rofstad, E.K. (2005). Intratumor heterogeneity in blood perfusion in orthotopic human melanoma xenografts assessed by dynamic contrast-enhanced magnetic resonance imaging. J. Magn. Reson. Imaging 21, 792-800.

Gillies, R.J., Schornack, P.A., Secomb, T.W., and Raghunand, N. (1999). Causes and effects of heterogeneous perfusion in tumors. Neoplasia 1, 197-207.

Griffiths, J.R. and Robinson, S.P. (1999). The OxyLite: a fibre-optic oxygen sensor. Br. J. Radiol. 72, 627-630.

Gulledge, C.J. and Dewhirst, M.W. (1996). Tumor oxygenation: a matter of supply and demand. Anticancer Res. 16, 741-749.

Gulliksrud, K., Brurberg, K.G., and Rofstad, E.K. (2009). Dynamic contrast-enhanced magnetic resonance imaging of tumor interstitial fluid pressure. Radiother. Oncol. 91, 107-113.

Gulliksrud, K., Mathiesen, B., Galappathi, K., and Rofstad, E.K. (2010). Quantitative assessment of hypoxia in melanoma xenografts by dynamic contrast-enhanced magnetic resonance imaging: intradermal versus intramuscular tumors. Radiother. Oncol. 97, 233-238.

Gulliksrud, K., Vestvik, I.K., Galappathi, K., Mathiesen, B., and Rofstad, E.K. (2008). Detection of different hypoxic cell subpopulations in human melanoma xenografts by pimonidazole immunohistochemistry. Radiat. Res. 170, 638-650.

Hall, E.J. and Giaccia, A.J. (2006). Radiobiology for the Radiologist. Lippinott Williams & Wilkins, Philadelphia. 6th ed.

Hanahan, D. and Weinberg, R.A. (2000). The hallmarks of cancer. Cell 100, 57-70.

Hanahan, D. and Weinberg, R.A. (2011). Hallmarks of cancer: the next generation. Cell 144, 646-674.

Heldin, C.H., Rubin, K., Pietras, K., and Ostman, A. (2004). High interstitial fluid pressure - an obstacle in cancer therapy. Nat. Rev. Cancer 4, 806-813.

Helmlinger, G., Yuan, F., Dellian, M., and Jain, R.K. (1997). Interstitial pH and pO_2 gradients in solid tumors in vivo: high-resolution measurements reveal a lack of correlation. Nat. Med. 3, 177-182.

Hendrick, R.E. and Haacke, E.M. (1993). Basic physics of MR contrast agents and maximization of image contrast. J. Magn. Reson. Imaging 3, 137-148.

Hittmair, K., Gomiscek, G., Langenberger, K., Recht, M., Imhof, H., and Kramer, J. (1994). Method for the quantitative assessment of contrast agent uptake in dynamic contrast-enhanced MRI. Magn. Reson. Med. 31, 567-571.

Höckel, M., Knoop, C., Schlenger, K., Vorndran, B., Baussmann, E., Mitze, M., Knapstein, P.G., and Vaupel, P. (1993). Intratumoral pO_2 predicts survival in advanced cancer of the uterine cervix. Radiother. Oncol. 26, 45-50.

Hoogsteen, I.J., Marres, H.A., van der Kogel, A.J., and Kaanders, J.H. (2007). The hypoxic tumour microenvironment, patient selection and hypoxia-modifying treatments. Clin. Oncol. (R. Coll. Radiol.) 19, 385-396.

Horsman, M.R. (1995). Nicotinamide and other benzamide analogs as agents for overcoming hypoxic cell radiation resistance in tumours. A review. Acta Oncol. 34, 571-587.

Horsman, M.R. (1998). Measurement of tumor oxygenation. Int. J. Radiat. Oncol. Biol. Phys. 42, 701-704.

Hsiang, D.J., Yamamoto, M., Mehta, R.S., Su, M.Y., Baick, C.H., Lane, K.T., and Butler, J.A. (2007). Predicting nodal status using dynamic contrast-enhanced magnetic resonance imaging in patients with locally advanced breast cancer undergoing neoadjuvant chemotherapy with and without sequential trastuzumab. Arch. Surg. 142, 855-861.

Hylton, N. (2006). Dynamic contrast-enhanced magnetic resonance imaging as an imaging biomarker. J. Clin. Oncol. 24, 3293-3298.

Jackson, A., O'Connor, J.P.B., Parker, G.J.M., and Jayson, G.C. (2007). Imaging tumor vascular heterogeneity and angiogenesis using dynamic contrast-enhanced magnetic resonance imaging. Clin. Cancer Res. 13, 3449-59.

Jain, R.K. (1988). Determinants of tumor blood flow: a review. Cancer Res. 48, 2641-2658.

Jain, R.K. (2008). Taming vessels to treat cancer. Sci. Am. 298, 56-63.

Jain, R.K. and Stylianopoulos, T. (2010). Delivering nanomedicine to solid tumors. Nat. Rev. Clin. Oncol. 7, 653-664.

Jang, A. and Hill, R.P. (1997). An examination of the effects of hypoxia, acidosis, and glucose starvation on the expression of metastasis-associated genes in murine tumor cells. Clin. Exp. Metastasis 15, 469-483.

Ke, Q. and Costa, M. (2006). Hypoxia-inducible factor-1 (HIF-1). Mol. Pharmacol. 70, 1469-1480.

Killion, J.J., Radinsky, R., and Fidler, I.J. (1998). Orthotopic models are necessary to predict therapy of transplantable tumors in mice. Cancer Metastasis Rev. 17, 279-284.

Konerding, M.A., Fait, E., and Gaumann, A. (2001). 3D microvascular architecture of pre-cancerous lesions and invasive carcinomas of the colon. Br. J. Cancer 84, 1354-1362.

Langley, R.R. and Fidler, I.J. (2011). The seed and soil hypothesis revisited--the role of tumor-stroma interactions in metastasis to different organs. Int. J. Cancer 128, 2527-2535.

Leach, M.O., Brindle, K.M., Evelhoch, J.L., Griffiths, J.R., Horsman, M.R., Jackson, A., Jayson, G., Judson, I.R., Knopp, M.V., Maxwell, R.J., McIntyre, D., Padhani, A.R., Price, P., Rathbone, R., Rustin, G., Tofts, P.S., Tozer, G.M., Vennart, W., Waterton, J.C., Williams, S.R., and Workman, P. (2003). Assessment of antiangiogenic and antivascular therapeutics using MRI: recommendations for appropriate methodology for clinical trials. Br. J. Radiol. 76, S87-S91.

Leo, C., Giaccia, A.J., and Denko, N.C. (2004). The hypoxic tumor microenvironment and gene expression. Semin. Radiat. Oncol. 14, 207-214.

Li, L.Z., Zhou, R., Zhong, T., Moon, L., Kim, E.J., Qiao, H., Pickup, S., Hendrix, M.J., Leeper, D., Chance, B., and Glickson, J.D. (2007). Predicting melanoma metastatic potential by optical and magnetic resonance imaging. Adv. Exp. Med. Biol. 599, 67-78.

Loiselle, C.R., Eby, P.R., Peacock, S., Kim, J.N., and Lehman, C.D. (2011). Dynamic contrast-enhanced magnetic resonance imaging and invasive breast cancer: primary lesion kinetics correlated with axillary lymph node extracapsular extension. J. Magn. Reson. Imaging 33, 96-101.

Loncaster, J.A., Carrington, B.M., Sykes, J.R., Jones, A.P., Todd, S.M., Cooper, R., Buckley, D.L., Davidson, S.E., Logue, J.P., Hunter, R.D., and West, C.M. (2002). Prediction of radiotherapy outcome using dynamic contrast enhanced MRI of carcinoma of the cervix. Int. J. Radiat. Oncol. Biol. Phys. 54, 759-767.

Lunt, S.J., Fyles, A., Hill, R.P., and Milosevic, M. (2008). Interstitial fluid pressure in tumors: therapeutic barrier and biomarker of angiogenesis. Future Oncol. 4, 793-802.

Milosevic, M., Fyles, A., Hedley, D., Pintilie, M., Levin, W., Manchul, L., and Hill, R. (2001). Interstitial fluid pressure predicts survival in patients with cervix cancer independent of clinical prognostic factors and tumor oxygen measurements. Cancer Res. 61, 6400-6405.

Milosevic, M.F., Fyles, A.W., and Hill, R.P. (1999). The relationship between elevated interstitial fluid pressure and blood flow in tumors: a bioengineering analysis. Int. J. Radiat. Oncol. Biol. Phys. 43, 1111-1123.

Milosevic, M.F., Fyles, A.W., Wong, R., Pintilie, M., Kavanagh, M.C., Levin, W., Manchul, L.A., Keane, T.J., and Hill, R.P. (1998). Interstitial fluid pressure in cervical carcinoma: within tumor heterogeneity, and relation to oxygen tension. Cancer 82, 2418-2426.

Min, Y., Ghose, S., Boelte, K., Li, J., Yang, L., and Lin, P.C. (2011). C/EBP-δ regulates VEGF-C autocrine signaling in lymphangiogenesis and metastasis of lung cancer through HIF-1α. Oncogene 30, 4901-4909.

Moulder, J.E. and Rockwell, S. (1984). Hypoxic fractions of solid tumors: experimental techniques, methods of analysis, and a survey of existing data. Int. J. Radiat. Oncol. Biol. Phys. 10, 695-712.

Newbold, K., Castellano, I., Charles-Edwards, E., Mears, D., Sohaib, A., Leach, M., Rhys-Evans, P., Clarke, P., Fisher, C., Harrington, K., and Nutting, C. (2009). An exploratory study into the role of dynamic contrast-enhanced magnetic resonance imaging or perfusion computed tomography for detection of intratumoral hypoxia in head-and-neck cancer. Int. J. Radiat. Oncol. Biol. Phys. 74, 29-37.

Nordsmark, M., Alsner, J., Keller, J., Nielsen, O.S., Jensen, O.M., Horsman, M.R., and Overgaard, J. (2001). Hypoxia in human soft tissue sarcomas: adverse impact on survival and no association with p53 mutations. Br. J. Cancer 84, 1070-1075.

Nordsmark, M. and Overgaard, J. (2000). A confirmatory prognostic study on oxygenation status and loco-regional control in advanced head and neck squamous cell carcinoma treated by radiation therapy. Radiother. Oncol. 57, 39-43.

Padera. T.P., Kadambi, A., di Tomaso, E., Carreira, C.M., Brown, E.B., Boucher, Y., Choi, N.C., Mathisen, D., Wain, J., Mark, E.J., Munn, L.L., and Jain, R.K. (2002). Lymphatic metastasis in the absence of functional intratumor lymphatics. Science 296, 1883-1886.

Paget, S. (1989). The distribution of secondary growths in cancer of the breast. 1889. Cancer Metastasis Rev. 8, 98-101.

Paldino, M.J. and Barboriak, D.P. (2009). Fundamentals of quantitative dynamic contrast-enhanced MR imaging. Magn. Reson. Imaging Clin. N. Am. 17, 277-289.

Pepper, M.S., Tille, J.C., Nisato, R., and Skobe, M. (2003). Lymphangiogenesis and tumor metastasis. Cell Tissue Res. 314, 167-177.

Poste, G. and Fidler, I.J. (1980). The pathogenesis of cancer metastasis. Nature 283, 139-146.

Rofstad, E.K. (1989). Hypoxia and reoxygenation in human melanoma xenografts. Int. J. Radiat. Oncol. Biol. Phys. 17, 81-89.

Rofstad, E.K. (1994). Orthotopic human melanoma xenograft model systems for studies of tumour angiogenesis, pathophysiology, treatment sensitivity and metastatic pattern. Br. J. Cancer 70, 804-812.

Rofstad, E.K. (2000). Microenvironment-induced cancer metastasis. Int. J. Radiat. Biol. 76, 589-605.

Rofstad, E.K. and Danielsen, T. (1999). Hypoxia-induced metastasis of human melanoma cells: involvement of vascular endothelial growth factor-mediated angiogenesis. Br. J. Cancer 80, 1697-1707.

Rofstad, E.K., Galappathi, K., Mathiesen, B., and Ruud, E.B. (2007). Fluctuating and diffusion-limited hypoxia in hypoxia-induced metastasis. Clin. Cancer Res. 13, 1971-1978.

Rofstad, E.K., Gaustad, J.V., Brurberg, K.G., Mathiesen, B., Galappathi, K., and Simonsen, T.G. (2009). Radiocurability is associated with interstitial fluid pressure in human tumor xenografts. Neoplasia 11, 1243-1251.

Rofstad, E.K., Gaustad, J.V., Egeland, T.A., Mathiesen, B., and Galappathi, K. (2010a). Tumors exposed to acute cyclic hypoxic stress show enhanced angiogenesis, perfusion and metastatic dissemination. Int. J. Cancer 127, 1535-1546.

Rofstad, E.K. and Halsør, E.F. (2000). Vascular endothelial growth factor, interleukin 8, platelet-derived endothelial cell growth factor, and basic fibroblast growth factor promote angiogenesis and metastasis in human melanoma xenografts. Cancer Res. 60, 4932-4938.

Rofstad, E.K. and Halsør, E.F. (2002). Hypoxia-associated spontaneous pulmonary metastasis in human melanoma xenografts: involvement of microvascular hot spots induced in hypoxic foci by interleukin 8. Br. J. Cancer 86, 301-308.

Rofstad, E.K. and Mathiesen, B. (2010). Metastasis in melanoma xenografts is associated with tumor microvascular density rather than extent of hypoxia. Neoplasia 12, 889-898.

Rofstad, E.K., Mathiesen, B., Kindem, K., and Galappathi, K. (2006). Acidic extracellular pH promotes experimental metastasis of human melanoma cells in athymic nude mice. Cancer Res. 66, 6699-6707.

Rofstad, E.K. and Måseide, K. (1999). Radiobiological and immunohistochemical assessment of hypoxia in human melanoma xenografts: acute and chronic hypoxia in individual tumours. Int. J. Radiat. Biol. 75, 1377-1393.

Rofstad, E.K., Rasmussen, H., Galappathi, K., Mathiesen, B., Nilsen, K., and Graff, B.A. (2002a). Hypoxia promotes lymph node metastasis in human melanoma xenografts by up-regulating the urokinase-type plasminogen activator receptor. Cancer Res. 62, 1847-1853.

Rofstad, E.K., Ruud, E.B., Mathiesen, B., and Galappathi, K. (2010b). Associations between radiocurability and interstitial fluid pressure in human tumor xenografts without hypoxic tissue. Clin. Cancer Res. 16, 936-945.

Rofstad, E.K., Steinsland, E., Kaalhus, O., Chang, Y.B., Hovik, B., and Lyng, H. (1994). Magnetic resonance imaging of human melanoma xenografts in vivo: proton spin-lattice and spin-spin relaxation times versus fractional tumour water content and fraction of necrotic tumour tissue. Int. J. Radiat. Biol. 65, 387-401.

Rofstad, E.K., Tunheim, S.H., Mathiesen, B., Graff, B.A., Halsør, E.F., Nilsen, K., and Galappathi, K. (2002b). Pulmonary and lymph node metastasis is associated with primary tumor interstitial fluid pressure in human melanoma xenografts. Cancer Res. 62, 661-664.

Schoppmann, S.F., Fenzl, A., Schindl, M., Bachleitner-Hofmann, T., Nagy, K., Gnant, M., Horvat, R., Jakesz, R., and Birner, P. (2006). Hypoxia inducible factor-1α correlates with VEGF-C expression and lymphangiogenesis in breast cancer. Breast Cancer Res. Treat. 99, 135-141.

Seierstad, T., Røe, K., and Høvik, B. (2007). Construction of a modified capacitive overlap MR coil for imaging of small animals and objects in a clinical whole-body scanner. Phys. Med. Biol. 52, N513-N522.

Semenza, G.L. (2003). Targeting HIF-1 for cancer therapy. Nat. Rev. Cancer 3, 721-732.

Semple, S.I., Harry, V.N., Parkin, D.E., and Gilbert, F.J. (2009). A combined pharmacokinetic and radiologic assessment of dynamic contrast-enhanced magnetic resonance imaging predicts response to chemoradiation in locally advanced cervical cancer. Int. J. Radiat. Oncol. Biol. Phys. 75, 611-617.

Steeg, P.S. (2006). Tumor metastasis: mechanistic insights and clinical challenges. Nat. Med. 12, 895-904.

Stubbs, M., McSheehy, P.M., Griffiths, J.R., and Bashford, C.L. (2000). Causes and consequences of tumour acidity and implications for treatment. Mol. Med. Today 6, 15-19.

Subarsky, P. and Hill, R.P. (2003). The hypoxic tumour microenvironment and metastatic progression. Clin. Exp. Metastasis 20, 237-250.

Sutherland, R.M., Rasey, J.S., and Hill, R.P. (1988). Tumor biology. Am. J. Clin. Oncol. 11, 253-274.

Talmadge, J.E., Singh, R.K., Fidler, I.J., and Raz, A. (2007). Murine models to evaluate novel and conventional therapeutic strategies for cancer. Am. J. Pathol. 170, 793-804.

Tatum, J.L., Kelloff, G.J., Gillies, R.J., Arbeit, J.M., Brown, J.M., Chao, K.S., Chapman, J.D., Eckelman, W.C., Fyles, A.W., Giaccia, A.J., Hill, R.P., Koch, C.J., Krishna, M.C., Krohn, K.A., Lewis, J.S., Mason, R.P., Melillo, G., Padhani, A.R., Powis, G., Rajendran, J.G., Reba, R., Robinson, S.P., Semenza, G.L., Swartz, H.M., Vaupel, P., Yang, D., Croft, B., Hoffman, J., Liu, G., Stone, H., and Sullivan, D. (2006). Hypoxia: importance in tumor biology, noninvasive measurement by imaging, and value of its measurement in the management of cancer therapy. Int. J. Radiat. Biol. 82, 699-757.

Taylor, J.S., Tofts, P.S., Port, R., Evelhoch, J.L., Knopp, M., Reddick, W.E., Runge, V.M., and Mayr, N. (1999). MR imaging of tumor microcirculation: promise for the new millennium. J. Magn. Reson. Imaging 10, 903-907.

Thomlinson, R.H. and Gray, L.H. (1955). The histological structure of some human lung cancers and the possible implications for radiotherapy. Br. J. Cancer 9, 539-549.

Tofts, P.S., Brix, G., Buckley, D.L., Evelhoch, J.L., Henderson, E., Knopp, M.V., Larsson, H.B., Lee, T.Y., Mayr, N.A., Parker, G.J., Port, R.E., Taylor, J., and Weisskoff, R.M. (1999). Estimating kinetic parameters from dynamic contrast-enhanced T(1)-weighted MRI of a diffusable tracer: standardized quantities and symbols. J. Magn. Reson. Imaging 10, 223-232.

Tredan, O., Galmarini, C.M., Patel, K., and Tannock, I.F. (2007). Drug resistance and the solid tumor microenvironment. J. Natl. Cancer Inst. 99, 1441-1454.

Tuncbilek, N., Tokatli, F., Altaner, S., Sezer, A., Türe, M., Omurlu, I.K., and Temizoz, O. (2011). Prognostic value DCE-MRI parameters in predicting factor disease free survival and overall survival for breast cancer patients. Eur. J. Radiol. In press.

Vaupel, P. (1990). Oxygenation of human tumors. Strahlenther. Onkol. 166, 377-386.

Vaupel, P. (2004). Tumor microenvironmental physiology and its implications for radiation oncology. Semin. Radiat. Oncol. 14, 198-206.

Vaupel, P., Kallinowski, F., and Okunieff, P. (1989). Blood flow, oxygen and nutrient supply, and metabolic microenvironment of human tumors: a review. Cancer Res. 49, 6449-6465.

Vaupel, P. and Mayer, A. (2007). Hypoxia in cancer: significance and impact on clinical outcome. Cancer Metastasis Rev. 26, 225-239.

Vestvik, I.K., Egeland, T.A., Gaustad, J.V., Mathiesen, B., and Rofstad, E.K. (2007). Assessment of microvascular density, extracellular volume fraction, and radiobiological hypoxia in human melanoma xenografts by dynamic contrast-enhanced MRI. J. Magn. Reson. Imaging 26, 1033-1042.

Walenta, S., Salameh, A., Lyng, H., Evensen, J.F., Mitze, M., Rofstad, E.K., and Mueller-Klieser, W. (1997). Correlation of high lactate levels in head and neck tumors with incidence of metastasis. Am. J. Pathol. 150, 409-415.

Walenta, S., Wetterling, M., Lehrke, M., Schwickert, G., Sundfor, K., Rofstad, E.K., and Mueller-Klieser, W. (2000). High lactate levels predict likelihood of metastases, tumor recurrence, and restricted patient survival in human cervical cancers. Cancer Res. 60, 916-921.

Weinmann, H.J., Brasch, R.C., Press, W.R., and Wesbey, G.E. (1984). Characteristics of gadolinium-DTPA complex: a potential NMR contrast agent. AJR Am. J. Roentgenol. 142, 619-624.

Wirtz, D., Konstantopoulos, K., and Searson, P.C. (2011). The physics of cancer: the role of physical interactions and mechanical forces in metastasis. Nat. Rev. Cancer 11, 512-522.

Wong, S.Y. and Hynes, R.O. (2006). Lymphatic or hematogenous dissemination: how does a metastatic tumor cell decide? Cell Cycle 5, 812-817.

Woodhouse, E.C., Chuaqui, R.F., Liotta, L.A. (1997). General mechanisms of metastasis. Cancer 80, 1529-1537.

Wouters, B.G., Weppler, S.A., Koritzinsky, M., Landuyt, W., Nuyts, S., Theys, J., Chiu, R.K., and Lambin, P. (2002). Hypoxia as a target for combined modality treatments. Eur. J. Cancer 38, 240-257.

Yankeelov, T.E. and Gore, J.C. (2009). Dynamic contrast enhanced magnetic resonance imaging in oncology: theory, data acquisition, analysis, and examples. Curr. Med. Imaging Rev. 3, 91-107.

Young, S.D., Marshall, R.S., and Hill, R.P. (1988). Hypoxia induces DNA overreplication and enhances metastatic potential of murine tumor cells. Proc. Natl. Acad. Sci. U.S.A. 85, 9533-9537.

Yuh, W.T., Mayr, N.A., Jarjoura, D., Wu, D., Grecula, J.C., Lo, S.S., Edwards, S.M., Magnotta, V.A., Sammet, S., Zhang, H., Montebello, J.F., Fowler, J., Knopp, M.V., and Wang, J.Z. (2009). Predicting control of primary tumor and survival by DCE MRI during early therapy in cervical cancer. Invest. Radiol. 44, 343-350.

Zahra, M.A., Hollingsworth, K.G., Sala, E., Lomas, D.J., and Tan, L.T. (2007). Dynamic contrast-enhanced MRI as a predictor of tumour response to radiotherapy. Lancet Oncol. 8, 63-74.

Zahra, M.A., Tan, L.T., Priest, A.N., Graves, M.J., Arends, M., Crawford, R.A., Brenton, J.D., Lomas, D.J., and Sala, E. (2009). Semiquantitative and quantitative dynamic contrast-enhanced magnetic resonance imaging measurements predict radiation response in cervix cancer. Int. J. Radiat. Oncol. Biol. Phys. 74, 766-773.

Zhong, H., De Marzo, A.M., Laughner, E., Lim, M., Hilton, D.A., Zagzag, D., Buechler, P., Isaacs, W.B., Semenza, G.L., and Simons, J.W. (1999). Overexpression of hypoxia-inducible factor 1alpha in common human cancers and their metastases. Cancer Res. 59, 5830-5835.

APPENDIX

ABBREVIATIONS AND SYMBOLS

AIF	arterial input function
CA	contrast agent
DCE-MRI	dynamic contrast enhanced magnetic resonance imaging
EC	endothelial cell
ECVF	extracellular volume fraction
EES	extravascular extracellular space
FGF	fibroblast growth factor
Gd-DTPA	gadolinium diethylene-triamine penta-acetic acid
HF_{Acu}	fraction of acutely hypoxic cells
HF_{Chr}	fraction of chronically hypoxic cells
HF_{Pim}	fraction of pimonidazole-positive cells
HF_{Rad}	fraction of radiobiologically hypoxic cells
HIF	hypoxia inducible factor
i.d.	intradermal
IFP	interstitial fluid pressure
IL-8	interleukin 8
i.m.	intramuscular
K^{trans}	the volume transfer constant (min^{-1}) of the contrast agent between blood plasma and the extravascular extracellular space
MVP	microvascular pressure
OER	oxygen enhancement ratio
PDGF	platelet-derived growth factor
pH_i	intracellular pH
pH_e	extracellular pH
pO_2	oxygen tension
SNR	signal to noise ratio
TCD_{50}	the dose at which 50% of the tumors are locally controlled
TGD	tumor growth delay

uPAR	urokinase-type plasminogen activator receptor
v_e	the fractional distribution volume of the contrast agent
VEGF	vascular endothelial growth factor

I

II

III

IV

V

VI